Influence of Electronic Delocalization in Metal-to-Ligand Charge Transfer Excited States

Geoffrey F. Strouse, Jon R. Schoonover, Richard Duesing,† Stephen Boyde, Wayne E. Jones, Jr., and Thomas J. Meyer*

Department of Chemistry, The University of North Carolina, Chapel Hill, North Carolina 27599−3290

Received August 11, 1994[⊗]

In the metal-to-ligand-charge transfer (MLCT) excited states of the ligand-bridged complexes $[(dmb)_2Ru(\mu\text{-bbpe})Ru(dmb)_2](PF_6)_4$ and $[(bpy)_2Os(\mu\text{-bbpe})Os(bpy)_2](PF_6)_4$ (bpy is 2,2′-bipyridine, dmb is 4,4′-dimethyl-2,2′-bipyridine, bbpe is *trans*-1,2-bis-(4-(4′-methyl)-2,2′-bipyridyl)ethene) bbpe acts as the acceptor ligand. This conclusion is based on transient UV−visible and resonance Raman measurements, which also reveal that the excited electron in the Ru complex is *delocalized* over the bbpe ligand. Compared to related complexes having comparable energy gaps, the lifetimes of $[(dmb)_2Ru(\mu\text{-bbpe})Ru(dmb)_2]^{4+*}$ ($\tau = 1.31$ μs in CH_3CN at 298 K) and $[(dmb)_2Ru(bbpe)]^{2+*}$ ($\tau = 1.15$ μs in CH_3CN at 298 K) are unusually long. The extended lifetimes are a delocalization effect caused by decreased bond displacement changes in the excited state. This decreases vibrational overlap between states, and the rate constant for nonradiative decay. Delocalization disperses the excited electron over the molecular framework of the acceptor ligand, decreasing changes in local bond displacements compared to bpy. These results have important implications for the design of complexes which are broad visible light absorbers and yet retain accessible excited state lifetimes.

Introduction

Decay of metal-to-ligand change transfer (MLCT) excited states of polypyridyl complexes of Ru^{II}, Os^{II}, and Re^{I} at room temperature in fluid solution are typically dominated by nonradiative processes.[1−4] Their rate constants typically *increase* as the energy gap between the ground and excited states *decreases*, consistent with the energy gap law.[1d,3a] Because of this effect, complexes with low energy absorption bands typically are weak emitters and have short-lived excited states. The decreased lifetimes limit their use as sensitizers in photoinduced electron and energy transfer.[5−8]

At the microscopic level the energy gap law arises from a quantum effect. The energy gap influences vibrational overlap between the initial and final states in the "acceptor modes".[3a,9−13] For these there is a change in equilibrium displacement (ΔQ_e)

† This paper is in memory of Dr. Richard Duesing. Rich obtained his Ph.D. in Chemistry from the University of North Carolina at Chapel Hill in 1990 and then took a postdoctoral position at Los Alamos National Laboratory. His tragic death in an automobile accident in November 1991 cut short a promising scientific career.

[⊗] Abstract published in *Advance ACS Abstracts,* December 1, 1994.

(1) (a) Juris, A.; Balzani, V.; Baragelletti, F.; Campagna, S.; Belser, P.; Von Zelewsky, A. *Coord. Chem. Rev.* **1988**, *84*, 85. (c) Krause, R. A. *Struct. Bonding (Berlin)* **1987**, *67*, 1. (d) Meyer, T. J. *Pure and Appl. Chem.* **1986**, *58*, 1576. (e) Kalayanasundaram, K. *Coord. Chem. Rev.* **1982**, *46*, 159. (f) Seddon, K. R. *Coord. Chem. Rev.* **1982**, *41*, 79. (g) Ferguson, J.; Herren, F.; Krausz, E. R.; Maeder, M.; Vrbancich, J.; *Coord. Chem. Rev.* **1985**, *64*, 21. (h) Sutin, N.; Creutz, C. *Pure Appl. Chem.* **1980**, *52*, 2717.

(2) (a) Johnson, S. R.; Westmoreland, T. D.; Caspar, J. V.; Barqawi, K. R.; Meyer, T. J. *Inorg. Chem.* **1988**, *27*, 3195. (b) Kober, E. M.; Marshall, J. C.; Dressick, W. J.; Sullivan, B. P.; Caspar, J. V.; Meyer, T. *J. Inorg. Chem.* **1985**, *24*, 2755. (c) Allen, G. H.; White, R. P.; Rillema, D. P.; Meyer, T. J. *J. Am. Chem. Soc.* **1984**, *106*, 2613. (d) Kober, E. M.; Sullivan, B. P.; Dressick, W. J.; Caspar, J. V.; Meyer, T. J. *J. Am. Chem. Soc.* **1980**, *102*, 1383.

(3) (a) Kober, E. M.; Caspar, J. V.; Lumpkin, R. S.; Meyer, T. J. *J. Phys. Chem.* **1986**, *90*, 3722. (b) Barqawi, K. R.; Llobet, A.; Meyer, T. J. *J. Am. Chem. Soc.* **1988**, *110*, 7751. (c) Rillema, D. P.; Taghdiri, D. G.; Jones, D. S.; Keller, C. D.; Worl, L. A.; Meyer, T. J.; Levy, H. *Inorg. Chem.* **1987**, *26*, 5787.

(4) (a) Leasure, R. M.; Sacksteader, L. A.; Nesselrodt, D.; Reitz, G. A.; Demas, J. N.; Degfraff, B. A. *Inorg. Chem.* **1991**, *30*, 1330. (b) Pankuch, B. J.; Lackey, D. E.; Crosby, G. A. *J. Phys. Chem.* **1980**, *84*, 2061. (c) Creutz, C.; Chou, M.; Netzel, L.; Okumura, M.; Sutin, N. S. *J. Am. Chem. Soc.* **1980**, *102*, 1309. (d) Malouf, G.; Ford, P. C. *J. Am. Chem. Soc.* **1977**, *99*, 7213.

(5) (a) Chen, P.; Duesing, R. D.; Graff, D.; Meyer, T. J. *J. Phys. Chem.* **1991**, *95*, 5850. (b) Danielson, E.; Elliot, C. M.; Merkert, J. W.; Meyer, T. J. *J. Am. Chem. Soc.* **1987**, *109*, 2519. (c) Westmoreland, T. D.; Schanze, K. S.; Neveux, P. E., Jr.; Danielson, E.; Sullivan, B. P.; Chen, P.; Meyer, T. J. *Inorg. Chem.*, **1985**, *24*, 2596.

(6) (a) Lee, E. J.; Wrighton, M. S. *J. Am. Chem. Soc.* **1991**, *113*, 8562. (b) Cooley, L. F.; Larson, S. C.; Elliott, C. M.; Kelly, D. F. *J. Phys. Chem.* **1991**, *95*, 10694. (c) Resch, U.; Fox, M. A. *J. Phys. Chem.* **1991**, *95*, 6169. (d) Haga, M.; Kiyoshi, I.; Boone, S. R.; Pierpont, C. G. *Inorg. Chem.* **1990**, *29*, 3795. (e) Perkins, T. A.; Humer, W.; Netzel, T. L.; Schanze, K. S. *J. Phys. Chem.* **1990**, *94*, 2229.

(7) (a) Ohno, T.; Yoshimura, A.; Prasad, D. R.; Hoffman, M. Z. *J. Phys. Chem.* **1991**, *95*, 4723. (b) Ohno, T.; Yoshimura, A.; Mataga, N. *J. Phys. Chem.* **1990**, *94*, 4871. (c) Kitamura, N.; Obati, R.; Kim, H.-B.; Tazuke, S. *J. Phys. Chem.* **1989**, *93*, 5764. (d) Navon, G.; Sutin, N. *Inorg. Chem.* **1974**, *13*, 2159.

(8) (a) Meyer, T. J. In *Photochemical Processes in Organized Molecular Systems, Kitamura,* N., Ed.; Elsevier: Amsterdam, 1991; p 133. (b) Balzani, V.; Scandola, F. *Supramolecular Photochemistry*; Ellis Horwood: Chiahester, England, 1991. (c) Photoinduced Electron Transfer, Vols. 1−3; Mattey, J., Ed. *Top. Curr. Chem.* **1991**, *159*. (d) Meyer, T. J. *Acc. Chem. Res.* **1989**, *22*, 163. (e) *Photoinduced Electron Transfer*; Fox, M. A., Chanon, M., Eds. Elsevier: New York, 1988. (f) Balzani, V. Sabbatini, N.; Scandola, F. *Chem. Rev.* **1987**, *86*, 319. (g) Balzani, V., Ed. *Supramolecular Photochemistry*; NATO ASI Series C214; Reidel: Dordecht, The Netherlands, 1987. (h) Petersen, J. D. *Coord. Chem. Rev.* **1985**, *64*, 261.

(9) (a) Gillispie, G. D.; Lim, E. C. *Chem. Phys. Lett.* **1979**, *63*, 193. (b) Griesser, H. J.; Wild, U. P. *Chem. Phys.* **1980**, *63*, 193. (c) Murata, S.; Iwanga, C.; Toda, T.; Hokuburn, H. *Chem. Phys. Lett.* **1972**, *13*, 101. (d) Dinur, U.; Scharf, B. J. *J. Phys. Chem.* **1983**, *79*, 1176. (e) Bixon, M.; Jortner, J.; *J. Chem. Phys.*, **1968**, *48*, 715. (f) Freed, F. R.; Jortner, J. *J. Chem. Phys.* **1970**, *52*, 6272. (g) Englman, R.; Jortner, J. *J. Mol. Phys.* **1970**, *18*, 145.

(10) Caspar, J. V. Ph.D. Dissertation. The University of North Carolina at Chapel Hill, 1982.

(11) (a) Lumpkin, R. S.; Meyer, T. J. *J. Phys. Chem.*, **1986**, *90*, 5307. (b) Johnson, S. R.; Westmoreland, T. D.; Caspar, J. V.; Barqawi, K. R.; Meyer, T. J. *Inorg. Chem.* **1988**, 3195. (c) Caspar, J. V.; Kober, E. M.; Sullivan, B. P.; Meyer, T. J. *J. Am. Chem. Soc.* **1982**, *104*, 630. (d) Capar, J. V.; Meyer, T. J. *Inorg. Chem.* **1983**, *22*, 2444. (e) Caspar, J. V.; Meyer, T. J. *J. Phys. Chem.* **1983**, *87*, 952.

(12) (a) Henry, B. R.; Siebrand, W. In *Organic Molecular Photophysics*; Birks, J., Ed.; Wiley: New York, 1973; Vol 1. (b) Fong, F. K.; *Top. Appl. Phys.* **1976**, 15. (c) Avouris, P.; Gelbart, W. M.; El-Sayed, M. A. *Chem. Rev.* **1977**, 793. (d) Freed, F. R., *Acc. Chem. Res.* **1978**, *11*, 74. (e) Heller, E. J.; Brown, R. C. *J. Chem. Phys.* **1983**, *79*, 336. (f) Freed, F. R., *Top. Curr. Chem.* **1972**, *31*, 65.

0020-1669/95/1334-0473$09.00/0

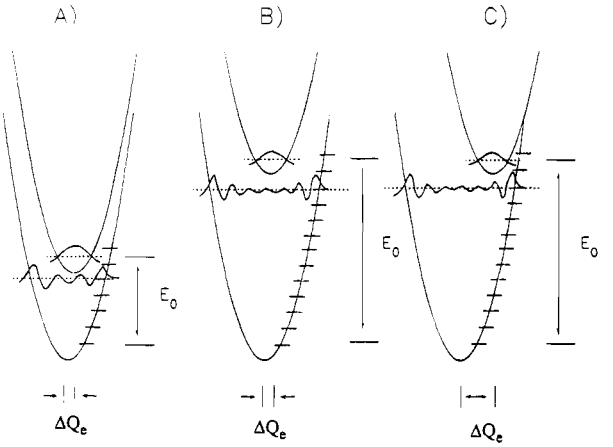

Figure 1. Potential energy diagram and associated vibrational wave functions (A) illustrating the effects of energy gap (B) and changes in equilibrium displacement (C) on vibrational wave function overlaps.

or frequency ($\nu = \omega/2\pi$) between the initial and final electronic states. The acceptor vibrations and solvent in the ground state accept the energy of the initial excited state. The rate constant for nonradiative decay (k_{nr}) increases as vibrational overlap increases.

As illustrated in Figure 1, both the energy gap and change in equilibrium displacement (ΔQ_e) influence vibrational overlap. As ΔQ_e increases, so does vibrational overlap and k_{nr}. This suggests a way to overcome a low energy gap, by decreasing ΔQ_e and structural distortion in the excited state.

In MLCT excited states, the excited electron occupies a π^* ligand orbital, eq 1, (bpy is 2,2′-bipyridine). On the basis of resonance Raman measurements a series of medium frequency ring stretching modes from 1000 to 1650 cm^{-1} act as the primary acceptor vibrations. Energy is accepted by low frequency modes and the solvent but to a lesser degree.[3a,14,15]

$$[Ru^{II}(bpy)_3]^{2+} \rightarrow [(bpy)_2Ru^{III}(bpy^{\bullet-})]^{2+*} \qquad (1)$$

Structure at the acceptor ligand is known to play a role in excited state lifetimes. Compared to bpy, phen (phen is 1,10-phenanthroline) complexes of Os^{II} having the same energy gap have systematically lower k_{nr}'s.[16,17] The ligand is more rigid and ΔQ_e smaller as shown by Franck–Condon analyses of emission spectral profiles.

Another way to decrease ΔQ_e is by delocalization. As the number of conjugated π-bonds is increased in organic radical anions, bond orders increase and bond distances decrease. This is true for linear conjugated polyenes, α,ω-diphenylpolyenes, or benzenoid hydrocarbons, including benzene, naphthalene, and anthracene.[18–20] This is a delocalization effect. As the added electron is dispersed over the π-bonding framework, more bonds are distorted and the average displacement change is decreased.

From comparisons between ground and excited state resonance Raman spectra and emission spectral fitting, it has been estimated that local −C=C−, −C=N− bond displacements increase by ~0.014 Å in $[Ru(bpy)_3]^{2+*}$.[3a,15] Derivatives of 2,2′-bipyridine have been prepared in which two bipyridyl units are linked by a saturated spacer or a spacer that creates a single, conjugated aromatic framework.[21,22] The latter feature and its implication for extended conjugation, delocalization and minimizing ΔQ_e led to the current study. We have prepared the olefin-linked, bis-2,2′-bipyridine derivative *trans*-1,2-bis-(4-(4′-methyl)-2,2′-bipyridyl)ethene (bbpe) and $[(dmb)_2Ru(\mu\text{-bbpe})Ru(dmb)_2]^{4+}$, $[Ru(dmb)_2(bbpe)]^{2+}$, $[(bpy)_2Os(\mu\text{-bbpe})Os(bpy)_2]^{4+}$, and $[Os(bpy)_2(bbpe)]^{2+}$ (dmb = 4,4′-dimethyl-2,2′-bipyridine, bpy = 2,2′-bipyridine). We find evidence in their photophysical properties for delocalization and dramatically extended lifetimes.

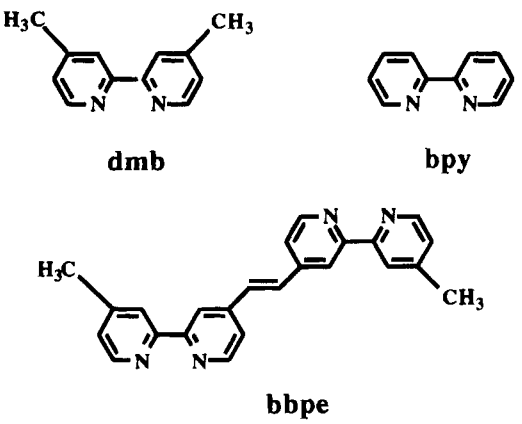

(13) (a) Lumpkin, R. S. Ph.D. Dissertation, The University of North Carolina at Chapel Hill, 1987. (b) Lumpkin, R. S.; Worl, L. A.; Murtaza, Z.; Meyer, T. J.; Kober, E. M. Manuscript in preparation. (c) Caspar, J. V.; Westmoreland, T. D.; Allen, G. H.; Bradley, P. G.; Meyer, T. J.; Woodruff, W. H. *J. Am. Chem. Soc.* **1984**, *106*, 3492. (d) Worl, L. A.; Duesing, R. D.; Chen, P.; della Ciana, L. D.; Meyer, T. J. *J. Chem. Soc., Dalton Trans.* **1991**, 849. (e) Shaver, R. J.; Rillema, D. P.; Woods, C. *J. Chem. Soc., Chem. Commun.* **1990**, 179. (f) Leasure, R. M.; Sacksteder, L. A.; Nesselrodt, D.; Reitz, G. A.; Demas, J. N.; DeGraff, B. A. *Inorg. Chem.* **1991**, *30*, 3722.

(14) (a) Dallinger, R. F.; Woodruff, W. H. *J. Am. Chem. Soc.* **1979**, *101*, 4391. (b) Bradley, P. G.; Kress, N.; Hornberger, B. A.; Dallinger, R. F.; Woodruff, W. H. *J. Am. Chem. Soc.* **1981**, *103*, 7441. (c) McClanahan, J.; Dallinger, R. F.; Holler, F. J.; Kincaid, J. R. *J. Am. Chem. Soc.* **1985**, *107*, 4853. (d) Mabrouk, P. A.; Wrighton, M. S. *Inorg. Chem.* **1986**, *25*, 526. (e) Yabe, T.; Orman, L. K.; Anderson, D. R.; Yu, S.-C.; Xu, X. Hopkins, J. B. *J. Phys. Chem.* **1990**, *94*, 7128. (f) Strouse, G. F.; Anderson, P. A.; Schoonover, J. R.; Meyer, T. J.; Keene, F. R. *Inorg. Chem.* **1992**, *31*, 3004. (g) Schoonover, J. R.; Strouse, G. F.; Meyer, T. J. Unpublished results.

(15) (a) Danzer, G. D.; Janusz, A. G.; Strommen, D. P.; Kincaid, J. R. *J. Raman Spectrosc.* **1990**, *21*, 3. (b) Strommen, D. P.; Mallick, P. K.; Danzer, G. D.; Lumpkin, R. S.; Kincaid, J. R. *J. Phys. Chem.* **1990**, *94*, 1357. (c) Mallick, P. K.; Danzer, G. D.; Strommen, D. P.; Kincaid, J. P. *J. Phys. Chem.* **1988**, *92*, 5628.

(16) Kober, E. M.; Caspar, J. V.; Lumpkin, R. S.; Meyer, T. J. *J. Phys. Chem.* **1986**, *90*, 3722.

(17) (a) Kumar, C. V.; Barton, J. K.; Turro, N. J.; Gould, I. R. *Inorg. Chem.* **1987**, *26*, 1455. (b) Kumar, C. V.; Barton, J. K.; Gould, I. R.; Turro, N. J.; Houten, J. V. *Inorg. Chem.* **1988**, *27*, 648. (c) Chang, Y. J.; Xu, X.; Yabe, T.; Yu, S.-C.; Anderson, D. R.; Orman, L. K.; Hopkins, J. B. *J. Phys. Chem.* **1990**, *94*, 729.

(18) (a) Van Duyne, R. P.; Suchanski, M. R.; Lakovits, J. M.; Siedle, A. R., Parks, K. D.; Cotton, T. M. *J. Am. Chem. Soc.* **1979**, *101*, 2832. (b) Jeanmarie, D. C.; Van Duyne, R. P. *J. Am. Chem. Soc.* **1976**, *98*, 4029.

(19) (a) Takahashi, C.; Maeda, S. *Chem. Phys. Let.* **1973**, *22*, 364. (b) Takahashi, C.; Maeda, S. *Chem. Phys. Let.* **1974**, *28*, 22. (c) Takahashi, C.; Maeda, S. *Chem. Phys. Let.* **1974**, *24*, 584.

(20) (a) Zahradník, R.; Cársky, P. *J. Phys. Chem.* **1970**, *74*, 1235. (b) Zahradník, R.; Cársky, P. *J. Phys. Chem.* **1970**, *74*, 1240. (c) Zahradník, R.; Cársky, P. *J. Phys. Chem.* **1970**, *74*, 1249.

(21) (a) Hunziker, M.; Ludi, A. *J. Am. Chem. Soc.* **1977**, *99*, 7370. (b) Dose, E. V.; Wilson, L. J.; *Inorg. Chem.* **1978**, *17*, 2660. (c) Rillema, D. P.; Mack, K. B. *Inorg. Chem.* **1982**, *21*, 3849. (d) Rillema, D. P.; Allen, G.; Meyer, T. J.; Conrad, D. *Inorg. Chem.* **1983**, *22*, 1617. (e) Sahai, R.; Baucom, D. A.; Rillema, D. P.; *Inorg. Chem.* **1986**, *25*, 3843. (f) Braunstein, C. H.; Baker, A. D.; Strekas, T. C.; Gafney, H. D. *Inorg. Chem.*, **1984**, *23*, 857. (g) Kohlmann, S.; Ernst, S.; Kaim, W. *Angew. Chem., Int. Ed. Engl.* **1985**, *24*, 684. (h) Kaim, W.; Ernst, S.; Kohlmann, S.; Welkerling, P. *Chem. Phys. Lett.* **1985**, *118*, 431. (i) Ernst, S.; Kasack, V.; Kaim, W. *Inorg. Chem.* **1988**, *27*, 1146. (j) Schmehl, R. H.; Auerbach, R. A.; Wacholtz, W. F.; Elliott, C. M.; Freitag, R. A.; Merkert, J. W. *Inorg. Chem.* **1986**, *25*, 2440. (k) Wacholtz, W. F.; Auerbach, R. A.; Schmehl, R. H. *Inorg. Chem.* **1987**, *26*, 2989. (l) Furue, M.; Kinoshita, S.; Kushida, T. *Chem. Lett.* **1987**, 2355. (m) Furue, M.; Kuroda, N.; Nozakura, S. *Chem. Lett.* **1986**, 1209.

Part of this work has appeared in a preliminary communication.[23]

Experimental Section

Materials. The reagents SeO_2 (Aldrich), *N*-bromosuccinimide (NBS) (Aldrich), and azobisisobutyronitrile (AIBN) (Kodak) were purified by literature methods prior to use.[24] The ligand 4-methyl-4′-vinyl-2,2′-bipyridine (vbpy) was prepared by a modified literature method where α,4-dichloroanisole was used in place of chloromethyl methyl ether.[25] The reagents 4,4′-dimethyl-2,2′-bipyridyl (dmb) and *N,N,N′,N′*-tetramethylbenzidine (TMBD), were used without further purification. $Ru(dmb)_2Cl_2$ and $Os(bpy)_2Cl_2$ was prepared by literature methods.[11a,26a] The model complexes, $[Ru(dmb)_3](PF_6)_2$, $[Ru(bpy)_2(py)Cl](PF_6)$, $[Ru(dmb)_2(vbpy)](PF_6)_2$, $[Os(dmb)_3](PF_6)_2$, $[Os(bpy)_2(py)_2](PF_6)_2$, and $[Os(bpy)_3](PF_6)$ were prepared previously.[26,27] All solvents used in the preparations were reagent grade and were used as supplied except where specified. Tetrahydrofuran (THF) was purified by distillation over Na/benzophenone and stored under argon. Spectral grade acetonitrile (Burdick and Jackson), methanol (Burdick and Jackson), and ethanol (freshly distilled over Mg/I_2) were used for all spectroscopic and electrochemical measurements. All metal complexes were purified by cation-exchange HPLC chromatography on a Brownlee CX-100 Prep 10 column by utilizing a 4 mM KBr, CH_3CN/KH_2PO_4 (pH = 7.0) buffered linear gradient controlled by a Perkin-Elmer Series 4 pump control unit and monitored at a Perkin-Elmer LC-95 variable UV−vis spectrophotometer detector fitted with a 4.5 μL pathlength flow cell. Metathesis of the Br^- salt to the PF_6^- salt was carried out by the addition of an aqueous solution of NH_4PF_6 prior to photophysical analysis. Chemical analyses were performed by either Galbraith Laboratories or Oneida Research Services.

Measurements. UV/vis spectra and near infrared measurements were obtained on CH_3CN solutions on a Cary 14 interfaced to an IBM PC by On-Line Systems, Inc. Absorption spectra in the near-IR region were measured on 10^{-3} M solutions in CD_3CN with a 650 W(120 V) tungsten−iodide lamp source at 60 V and a PbS detector. IR spectra were recorded on samples prepared as Nujol mulls between NaCl plates on a Nicolet 20DX FT-IR spectrometer. ^1H NMR spectra were recorded on Varian XL-400 or Brüker AC200 spectrometers. Corrected emission spectra were recorded on a Spex Fluorolog-2 emission spectrometer equipped with a 450 W xenon lamp and cooled 10-stage Hamamatsu R928 or R664 photomultipliers. Optical response characteristics for the Spex Flurolog and PMT tube response were corrected with a calibration curve generated with 2.0 mm slits by using a NIST calibrated 250 W Ze lamp (Optronics Laboratories, Inc. Model 220M), controlled by a precision current source at 6.50W (Optronics Laboratories, Inc. Model 65). Room temperature spectra were obtained in 1-cm pathlength quartz cells for CH_3CN solutions at 298 ± 2 K. Spectra were obtained at 77 K in 4:1 EtOH/MeOH (V:V) glasses immersed in liquid N_2 in a quartz finger dewar. Low temperature (150−290 K) spectra were obtained by using either a Janis NDT-6 cryostat controlled by a Lakeshore DRC-84C temperature controller or an Oxford DN1704 cryostat controlled by an Oxford DTC-2 temperature controller. Temperatures were equilibrated for 30−45 min and monitored with an external temperature probe (±3 K).

Emission quantum yields (ϕ_{em}) were measured relative to $[Ru(bpy)_3](PF_6)_2$ in CH_3CN ($\phi'_{em} = 0.062$) and were calculated by eq 2.[28a] In eq

$$\phi_{em} = \phi'_{em}\left(\frac{I}{I'}\right)\left(\frac{A'}{A}\right)\left(\frac{n}{n'}\right)^2 \qquad (2)$$

2, I (sample) and I' (standard) are the integrated emission intensities, A and A' the absorbances at the excitation wavelength, and n and n' the refractive indices of the solvents.

Photochemical quantum yields for ligand loss (ϕ_p) were measured relative to $[Ru(bpy)_3](PF_6)_2$ ($\phi_p \sim 0.029$) on 1.0×10^{-5} M samples. The samples were dissolved in freeze−pump−thaw degassed (4×), stirred 2 mM $[N(n\text{-}C_4H_9)_4]Cl/CH_3CN$ solutions in a 1-cm quartz cell in a temperature-controlled cell holder at 295 K with a Lauda RM-6 variable temperature water bath. Excitation at 452 nm was achieved with a collimated 75 W Xe lamp powered by a PTI-LPS-220 arc power supply attached to a PTI-A-1010 *f4* matched monochromator with a 1200 lines/mm grating blazed at 500 nm. The intensity of the source was measured by using Reinecke salt as a chemical actinometer.[28c] The value of ϕ_p was calculated, eq 3, by monitoring the loss of emission

$$\phi_p = \frac{R_t}{I_0(1 - 10^{-A_0})} \qquad (3)$$

intensity as a function of time (12 h). In this equation, I_0 is the irradiance intensity of the source, R_t is the slope of a plot of emission intensity versus time at λ_{em}, and A_0 is the initial absorbance of the sample at the excitation wavelength.[28]

Time-resolved emission measurements were made by using a PRA LN 1000/LN102 nitrogen laser/dye laser combination for sample excitation. The emission was monitored at a right angle to the excitation source by using a PRA B204-3 monochromator with a cooled, 10-stage, Hamamatsu R928 PMT. Transient absorption difference spectra were measured by using a PDL-2 pulsed dye laser (Coumarin 460 dye) pumped by a Quanta-Ray DCR-2A Nd-YAG laser with an excitation pulse of ~6 ns at <5 mJ/pulse. The excitation beam was coincident to an Applied Photophysics laser kinetic spectrometer, which utilized a 250 W pulsed Xe arc as a probe beam, quartz optics, a *f*/3.4 grating monochromator, and a 5-stage, cooled PMT. The outputs for the laser experiments were coupled to either a LeCroy 9400 digital oscilloscope or a LeCroy 6880 digitizer interfaced to an IBM PC. The measurements were made on argon sparged CH_3CN solutions (1×10^{-5} M) in 1-cm pathlength square cuvettes. Transient emission and absorption data were fit by utilizing a global minimization routine based on a modified Levenberg−Marquardt nonlinear, least squares iterative fitting routine.[29]

Resonance Raman spectra were obtained on ~10^{-3} M samples in CH_3CN or CH_2Cl_2 at 298 K. The spectra were acquired on spinning samples by using a 135° backscattering geometry. Laser excitation was supplied by a Spectra-Physics 165−05 Ar^+ or a Coherent INNOVA 90 K Kr^+ laser. The scattered radiation was dispersed by a Jobin Yvon U1000 (Instruments SA) double monochromator and detected by a thermoelectrically cooled Hamamatsu R943-02 photomultiplier tube. The resulting signal was processed by a Spectra Link photon counting system (Instruments SA). Data acquisition was controlled by an IBM PS-2 Model 80 computer with Enhanced Prism software (Instruments SA). Raman bands of the solvent served as internal frequency and intensity references.

Transient Raman spectra were measured by using the third harmonic (354.7 nm) of a Quanta-Ray DCR-2A pulsed Nd:YAG laser as the excitation source as well as the source for the Raman scattering. The samples (~10−20 mM) were degassed by three cycles of freeze−pump−thawing and sealed in an NMR tube. The scattered radiation was collected in a 135^0 backscattering geometry into a SPEX 1877 triplemate spectrometer equipped with an 1800 grooves/mm grating. The signal was detected by a Princeton Instrument's IRY-700G Optical Multichannel Analyzer operating in the gated mode with a ST-110 OSMA detector controller. Timing was controlled by a Princeton

(22) Creutz, C. *Prog. Inorg. Chem.* **1983**, *30*, 1.
(23) Boyde, S.; Strouse, G. F.; Jones, W. E.; Meyer, T. J. *J. Am. Chem. Soc.* **1990**, *112*, 7395.
(24) Perrin, D. D.; Armarego, W. L. F.; Perrin, D. R. *Purification of Laboratory Chemicals*, 2nd ed.; Pergamon: Oxford, England, 1980.
(25) Abruña, H. D.; Breikss, A. J.; Collum, D. B. *Inorg. Chem.* **1985**, *24*, 987.
(26) (a) Sprintschnik, G.; Sprintschnik, H. W.; Whitten, D. G. *J. Am. Chem. Soc.* **1976**, *98*, 2337. (b) Vining, W.; Caspar, J. V.; Meyer, T. J. *J. Phys. Chem.* **1985**, *89*, 1095. (c) Caspar, J. V.; Kober, E. M.; Sullivan, B. P.; Meyer, T. J. *J. Am. Chem. Soc.* **1982**, *104*, 630. (d) Kober, E. M.; Caspar, J. V.; Sullivan, B. P.; Meyer, T. J. *Inorg. Chem.* **1988**, *27*, 4587.
(27) (a) Kober, E. M.; Sullivan, B. P.; Dressick, W. J.; Caspar, J. V.; Meyer, T. J. *J. Am. Chem. Soc.* **1980**, *102*, 7313. (b) Wacholtz, W. A.; Auerbach, R. A.; Schmehl, R. H. *Inorg. Chem.* **1986**, *25*, 227.
(28) (a) Caspar, J. V.; Meyer, T. J. *J. Am. Chem. Soc.* **1983**, *106*, 5583. (b) Durham, B.; Caspar, J. V.; Nagle, J. K.; Meyer, T. J. *J. Am. Chem. Soc.* **1982**, *104*, 4803. (c) Wegner, E. E.; Adamson, A. W. *J. Am. Chem. Soc.* **1966**, *88*, 394.
(29) Danielson, E. Unpublished results.

Instrument's FG-100 pulse generator. The final spectra were the result of 16 min total integration times. Laser power was between 3 and 5 mJ per pulse. Data collection and storage were controlled by an IBM AT by using Princeton Instrument's software.

Electrochemical measurements were carried out in a N_2 drybox by using a EG&G PAR Model 173 potentiostat and Model 175 waveform generator or a EG&G PAR model 273 potentiostat. Potentials were measured with a 1-cm diameter Pt disk electrode relative to $Ag/AgNO_3$ (0.1M). The measured potential under identical conditions for the ferrocenium/ferrocene couple in CH_3CN (0.1 M $[N(n\text{-}C_4H_9)_4](PF_6)$) was +0.09 V. The generation of the radical anion of bbpe was carried out in K^0/benzophenone-dried THF (0.1 M $LiClO_4$) at a Pt gauze electrode at −2.20 V versus $Ag/AgNO_3$ (0.1 M). Electrochemical generation of the reduced form of $[(bpy)_2Os(\mu\text{-bbpe})Os(bpy)_2](ClO_4)_4$ was carried out at a Pt gauze electrode at −1.1 V vs $Ag/AgNO_3$ (0.1 M) in dimethoxyethane (DME) 0.2 M $[N(C_2H_5)_4](ClO_4)$. The DME was distilled from Na^0/benzophenone followed by distillation from Na^0.

Spectroelectrochemical measurements were conducted in an optically transparent thin layer (OTTL) cell prepared in a N_2 drybox and sealed via stopcocks. The cell utilized a 2 mm pathlength cuvette fitted with a Pt gauze working electrode, and a silver wire reference electrode. A Pt auxiliary was attached to the cell via a ground glass joint fitted with a fritted glass end. Electrochemical potentials for reduction were chosen 100 mV negative of E_p. Absorption spectra were collected as a function of time at a controlled potential on a Hewlett-Packard 8452A spectrophotometric diode array instrument coupled to an IBM-PC for data acquisition.

Analysis. Franck−Condon analyses of emission spectral profiles were conducted by using a two mode fitting program described previously, eq 4.[13] The emission spectra were converted to an abcissa linear in energy.[30] From resonance Raman studies, on bpy complexes, the medium frequency mode of quantum spacing, $\hbar\omega_M$, and electron-vibrational coupling constant, S_M, are averages of contributions from a series of ν(bpy) ring stretching modes from 1000 to 1600 cm^{-1}.[3a,14a−d,15] In the fits the average quantum spacing for these modes was constrained to be in the ranges 1350−1400 300−400 cm^{-1}. The $\hbar\omega_L$ and S_L are averaged quantities for a series of coupled low frequency modes.[3a,13] The contribution from the solvent is included in the band width $\Delta\bar{\nu}_{1/2}$. In order to fit the spectra to eq 4, the summations were carried out over five vibrational levels for $\hbar\omega_M$ ($\nu_M = 0$ to $\nu_M = 5$) and over 15 for $\hbar\omega_L$.

$$I(\bar{\nu}) = \sum_{\upsilon_M}^{5}\sum_{\upsilon_L}^{15}[(E_{00} - \upsilon_M\hbar\omega_M - \upsilon_L\hbar\omega_L/E_{00})^3(S_M{}^{\upsilon_M}/\upsilon_M!)] \times (S_L{}^{\upsilon_L}/\upsilon_L!)[\exp-\{4(\ln 2)(\bar{\nu} - E_{00} + \nu_M\hbar\omega_M + \upsilon_L\hbar\omega_L/\Delta\bar{\nu}_{1/2})^2\}] \quad (4)$$

In eq 4, the quantity $I(\bar{\nu})$ is the ratio of the intensity of the emission at energy $\bar{\nu}$ in cm^{-1} to the intensity maximum. The vibronic transitions were approximated as Gaussians having a full width at half-maximum (fwhm) of $\Delta\bar{\nu}_{1/2}$. The Gaussians were scaled in relative intensity by the term $S^{\upsilon}/\upsilon!$ and summed to generate the Franck−Condon envelope weighted by $\bar{\nu}^3$. The mathematical simulation generated the emission spectra in units of quanta emitted per unit energy.

The quantity E_{00} is the difference in energy between the ground and excited states in their $\nu = 0$ vibrational levels. It is related to the true 0−0 energy of the excited state, $E(0\text{−}0)$, by $E(0\text{−}0) = E_{00} + \lambda_0$ where λ_0 is the solvent reorganizational energy. The electron-vibrational coupling constants (Huang−Rhys factors) are dimensionless quantities related to the difference in equilibrium displacement for the normal modes (ΔQ_e) between the ground state and excited state by eq 5. In

$$S = {}^1/_2(M\omega/\hbar)(\Delta Q_e)^2 \quad (5)$$

this equation M is the reduced mass, and ω the angular frequency ($2\pi\nu$).

Estimates for $\hbar\omega_M$ were taken from the vibrational spacings that appear in low emperature glasses. Inclusion of the $S_L\hbar\omega_L$ term was required in order to obtain reasonable fits; however, S_L and $\hbar\omega_L$ are strongly correlated and can not be determined independently from the fits.

In fitting the room temperature spectra, E_{00}, S_M, and $\Delta\bar{\nu}_{1/2}$ were taken to be temperature dependent. It was also necessary to include "hot band" contributions from levels above $\upsilon_L{}^* = 0$ in the excited state at room temperature by inclusion of the term $I(\upsilon_L{}^*)$ in eq 6, which serves to broaden the spectrum.[13a,b] The $I(\upsilon_L{}^*)$ terms are the products of the Laguerre polynomial defined in eq 7 and a Boltzman population factor.

$$I(\upsilon_L{}^*) = \exp\left[\frac{-\hbar\omega_L}{k_BT}\right]I(\upsilon_L{}^* = 0) \quad (6)$$

$$I(n) = S^n\sum_{j=0}^{\infty}\left(\frac{x^j j!}{(n+j)!}\right)\left[\sum_{k=0}^{j}\left(\frac{(j+n)!}{(j-k)!(n+k)!}\right)\frac{(-S)^k}{k!}\right]^2 \quad (7)$$

AM1 Calculations. Semiempirical molecular orbital calculations, which utilized Dewar's AM1 orbital basis sets for C, H, and N were conducted on the AM1 molecular orbital package of Sybyl v5.41 on a VAX computer interfaced to an IBM-PC using Term Nitro 5.41 as a terminal emulator. Standard AM1 Gaussian core repulsion functions were implemented for repulsion terms between heteroatoms. Initial estimates for the C,H,N bond angles and distances were obtained from the crystal structures of $[Ru(dmb)_3](PF_6)_2$ and $[Ru(bpy)_3](PF_6)_2$.[31] The N−N tetrahedral angles for the bipyridyl halves of bbpe and $bbpe^{\bullet-}$ were fixed according to the crystal data; all other bond angles were allowed to minimize to the equilibrated geometry by a full cartesian gradient optimization.[32,33] The optimized bbpe and $bbpe^{\bullet-}$ ligand structures and energy levels were obtained by the convergence of the minimized ligand structure starting either from a localized ligand π-system or a fully conjugated ligand π-system. The molecular structures were calculated with a net charge of 0 for the neutral, and a net charge of −1 for the anions. Structural representations of the ligands in Figure 3 were generated from the minimized AM1 output files by importing the minimized Cartesian coordinate files into ChemDraw 3D.

Synthesis. Preparation of 4′-Methyl-2,2′-bipyridyline-4-carbaldehyde (1). The compound 4,4′-dimethyl-2′,2′-bipyridyl (dmb) (1.8 g, 9.68 mmol) and SeO_2 (1.1 g, 9.9 mmol) were added to 1,4-dioxane (50 mL) and the mixture was heated at reflux under an Ar atmosphere for 24 h. The solution was filtered while hot to remove precipitated Se, cooled to room temperature, and allowed to stand for 1 h. Filtration removed a pale yellow precipitate of 4′-methyl-2,2′-bipyridine-4-carboxylic acid. The filtrate was evaporated to dryness and the residue redissolved in ethyl acetate (500 mL). The ethyl acetate solution was treated with aqueous Na_2CO_3 (0.1 M, 20 mL) to remove residual carboxylic acids and extracted with a 0.2 M aqueous solution of sodium bisulfite (3 × 30 mL). The combined aqueous extracts were adjusted to pH 9 by the addition of Na_2CO_3 and reextracted with CH_2Cl_2 (3 × 30 mL). The CH_2Cl_2 extracts were combined and evaporated to dryness to give 4′-methyl-2,2′-bipyridine-4-carbaldehyde (**1**) (0.82 g., 43% yield) as a white powder. Anal. Calcd for $C_{12}H_{10}N_2O$: C, 72.7; H, 5.1; N, 14.1. Found: C, 72.6; H, 5.2; N, 14.0. MS: *m/e* 198 (calculated 198.22). IR (Nujol): ν(C=O) 1706 cm^{-1} (s). ^1H NMR (δ (ppm), $CDCl_3$): 2.44 (3H, s); 7.18 (1H, d); 7.68 (1H, d); 8.24 (1H, s); 8.57 (1H, d); 8.81 (1H, s); 8.85 (1H, d); 10.15 (1H, s).

Preparation of 4-(Bromomethyl)-4′-methyl-2,2′-bipyridine (2). This compound was prepared as described previously.[34] Purification was accomplished by redissolving the crude product in toluene and chromatographing the material by vacuum chromatography on silica gel (Kieselgel 60G) with 9:1 (v/v) toluene/CH_3CN. The desired product eluted as the second major band. The fractions containing the pure product were combined and evaporated to dryness to give **2** (0.75 g,

(30) Parker, C. A.; Rees, W. T. *Analyst* **1960**, *85*, 587.

(31) (a) Biner, M.; Bürgi, H. B.; Ludi, A.; Röhr, C. *J. Am. Chem. Soc.* **1992**, *114*, 5197. (b) Rillema, D. P.; Jones, D. S.; Levy, H. A. *J. Chem. Soc., Chem. Commun.* **1979**, 849.

(32) Dewar, M. J. S.; Zoebisch, E. G.; Healy, E. F.; Stewart, J. P. *J. Am. Chem. Soc.* **1985**, *107*, 3902.

(33) (a) Konig, E.; Kremer, S. *Chem. Phys. Lett.* **1970**, *5*, 877. (b) Orgel, L. E. *J. Chem. Soc.*, **1961**, 3683. (c) McPherson, A. M.; Fieselmann, B. F.; Lichtenberger, D. L.; McPherson, G. L.; Stucky, G. D. *J. Am. Chem. Soc.* **1979**, *101*, 3425. (d) Mayoh, B.; Day, P. *Theor. Chim. Acta* **1978**, *49*, 259.

(34) Gould, S.; Strouse, G. F.; Meyer, T. J.; Sullivan, B. P. *Inorg. Chem.* **1991**, 2942.

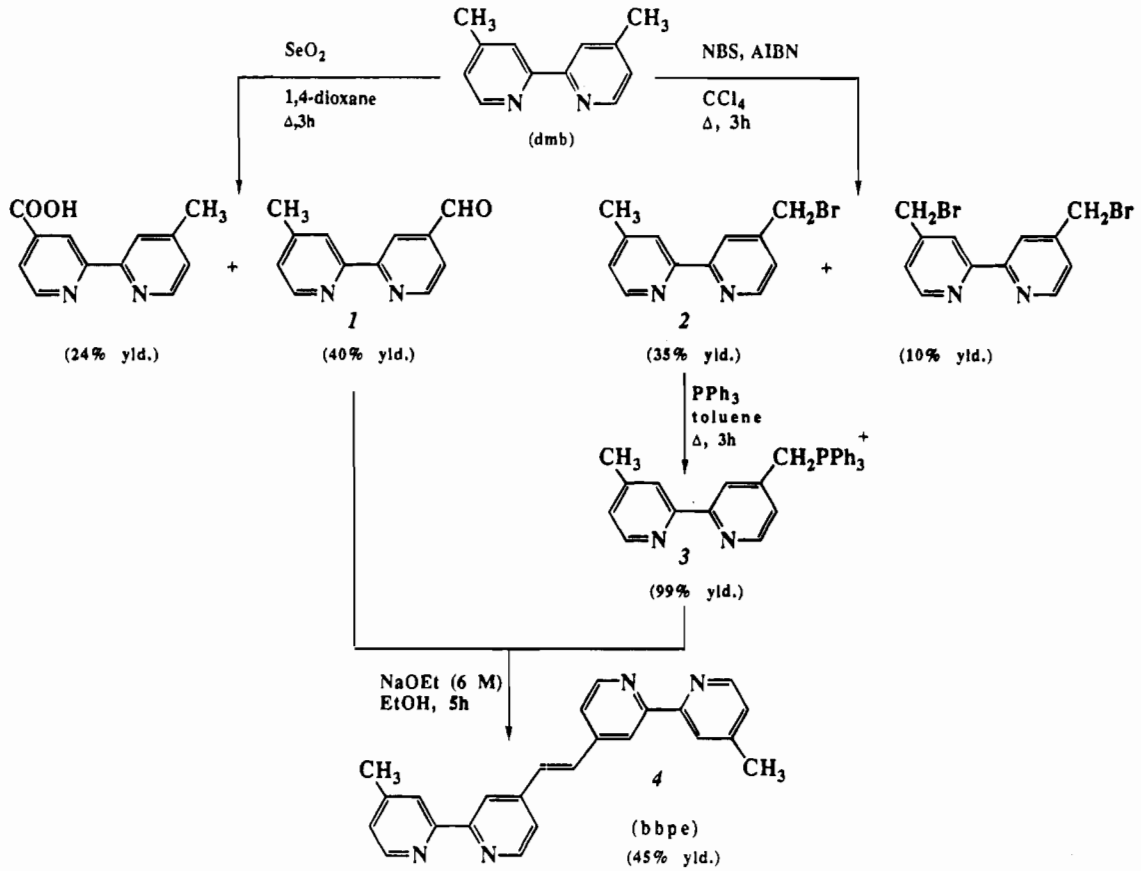

Figure 2. Synthetic strategy for the preparation of *trans*-1,2-bis(4′-methyl-2,2′-bipyrid-4-yl)ethene) (bbpe).

30% yield), as a white solid. The sample is sensitive to polar solvents and temperature, and so was stored under petroleum ether at 0 °C. ^{1}H NMR (δ (ppm), $CDCl_3$): 2.40 (3H, s); 4.42 (2H, s); 7.08 (1H, d); 7.25 (1H, d); 8.19 (1H, s); 8.35 (1H, s); 8.48 (1H, d); 8.62 (1H, d)).

Preparation of ((4-(4′-Methyl)-2,2′-bipyridyl)methyl)triphenylphosphonium Bromide (3). Compound **2** (0.5 g, 1.9 mmol) and excess PPh_3 (5 g, 19 mmol) were added to toluene (20 mL) and the solution heated at 60 °C for 2 h. The mixture was cooled to room temperature and filtered to yield 0.9 g of the triphenylphosphonium bromide salt, **3**, which was used without further purification. ^{1}H NMR (δ (ppm), DMSO): 2.61 (3H, s); 5.51 (1H, s); 5.58 (1H, s); 7.16 (1H, d); 7.38 (1H, d); 7.86 (12H, m); 8.00 (3H, d); 8.19 (1H, s); 8.26 (1H, s); 8.52 (1H, d); 8.63 (1H, d).

Preparation of 1,2-Bis(4-(4′-methyl)-2,2′-bipyridyl)ethene (bbpe) (4). Compounds **1** (0.110 g, 0.56 mmol) and **3** (0.335 g, 0.64 mmol) were dissolved in EtOH (20 mL) and stirred under Ar at 0 °C for 20 min. A solution of 0.3 M NaOEt/EtOH (2 mL) was added dropwise over a 2 min period, and the solution was allowed to warm to room temperature. After 5 h the volume was reduced to *ca.* 10 mL by evaporation under reduced pressure and H_2O (5 mL) was added. The mixture was filtered to isolate bbpe as a white powder which was washed with 1:1 H_2O/EtOH and dried under vacuum (93 mg, 45% yield after recrystallization from MeOH). Anal. Calcd for $C_{24}H_{20}N_4$: C, 79.0; H, 5.5; N, 15.4. Found: C, 79.0; H, 5.4; N, 15.5. MS: *m/e* 364 (calculated 364.69). ^{1}H NMR. (δ (ppm), $CDCl_3$): 2.42 (6H, s); 7.15 (2H, d); 7.38 (2H, d); 7.42 (2H, s); 8.23 (2H, s); 8.53 (2H, d); 8.56 (2H, s); 8.65 (2H, d). UV/Vis; ($CHCl_3$, λ_{max}, ϵ): 252 nm (2.2×10^4); 290 nm (2.93×10^4); 305 nm (sh).

Preparation of [(dmb)$_2$Ru(μ-bbpe)Ru(dmb)$_2$](PF$_6$)$_4$. The complex $[Ru(dmb)_2Cl_2]$ (0.11 g, 0.20 mmol) was added to ethylene glycol (10 mL) and heated at reflux for 5 min. The solution was cooled to 60 °C, bbpe (0.03 g, 0.08 mmol) was added, and the solution was stirred at 60 °C for 2 h. A saturated solution of $[NH_4][PF_6]$ (30 mL) was added dropwise and the resulting powdery red precipitate collected by filtration. The red powder was purified by size-exclusion chromatography on Sephadex LH-20 eluted with a 4:4:1 mixture of acetone/CH_2Cl_2/MeOH. It was reprecipitated by the addition of Et_2O. The final yield was 130 mg, 85% based on bbpe. Anal. Calcd for $C_{72}H_{72}N_{12}Ru_2P_4F_{24}$: C, 45.82; H, 3.85; N, 8.91. Found: C, 45.6; H, 3.6; N, 8.74. ^{1}H NMR (δ (ppm), DMSO-d_6): 2.48 (24H); 2.55 (6H); 7.3−7.8 (24H, overlapping multiplets); 7.9 (2H); 8.34 (8H); 8.45 (2H); 8.56 (2H); 8.65 (2H).

The salt $[Ru(dmb)_2(bbpe)](PF_6)_2.2H_2O$, was prepared as above except that 1 equiv of $[Ru(dmb)_2Cl_2]$ was added dropwise over the course of 1 h to a solution containing a 10-fold excess of bbpe in ethylene glycol at 60 °C. The final yield was 75%. Anal. Calcd for $C_{44}H_{44}N_8RuP_2F_{12}$: C, 47.53; H, 4.35; N, 10.08. Found: C, 47.05; H, 4.40; N, 9.82. ^{1}H NMR (δ (ppm), CD_3CN): 2.4−2.7 (18H); 7.1−8.0 (18H); 8.2−8.8 (10H).

Preparation of [(bpy)$_2$Os(μ-bbpe)Os(bpy)$_2$](PF$_6$)$_4$·2H$_2$O. The complex $[(Os(bpy)_2Cl_2]$ (0.30g, 0.52 mmol) was added to a solution containing bbpe (0.092 g, 0.25 mmol) in 40 mL of 1:1 ethylene glycol/H_2O (v:v) and heated at reflux for 5 h under Ar. To the solution was added 40 mL of a saturated solution of aqueous NH_4PF_6, resulting in a green precipitate which was collected by filtration. The green powder was purified by size-exclusion chromatography on Sephadex LH-20 eluted with a 4:4:1 mixture of acetone/CH_2Cl_2/MeOH. It was reprecipitated by the addition of Et_2O. The final yield was 0.29 g, 60% based on bbpe. Anal. Calcd for $C_{642}H_{56}N_{12}O_2Os_2P_4F_{24}$: C, 38.72; H, 2.84; N, 8.47. Found: C, 38.67; H, 2.62; N, 8.31. ^{1}H NMR (δ (ppm), CD_3CN): 2.70 (s, 6H), 7.20 (d, 2H), 7.3−7.55 (multiplet, 12H), 7.6−7.8 (multiplet, 12H), 7.8−8.0 (multiplet, 6H), 8.4−8.6 (multiplet, 8H).

The salt $[Os(dmb)_2(bbpe)](PF_6)_2$, was prepared as above except that 1 equiv of $[Os(bpy)_2Cl_2]$ was added dropwise over the course of 2 h to a refluxing solution of a 10-fold excess of bbpe in dimethoxyethane. The final yield was 52%. Anal. Calcd for $C_{40}H_{36}N_8OsP_2F_{12}$: C, 41.96; H, 3.52; N, 9.79. Found: C, 41.05; H, 3.73; N, 10.0. ^{1}H NMR (δ (ppm), CD_3CN): ^{1}H NMR. (δ (ppm), d_3-CD_3CN): 2.6−2.7 (6H); 7.1−8.0 (22H); 8.2−8.8 (10H).

Purification of Metal Complexes. Cation exchange HPLC was used to separate dimeric (+4) from monomeric (+2) cations on a Brownlee CX-100, Prep-10 HPLC column. The material was loaded onto the HPLC in 3:2 (v:v) CH_3CN/H_2O (phosphate buffered at pH 7.2) and eluted with a linear gradient of 4 mM KBr in the phosphate-

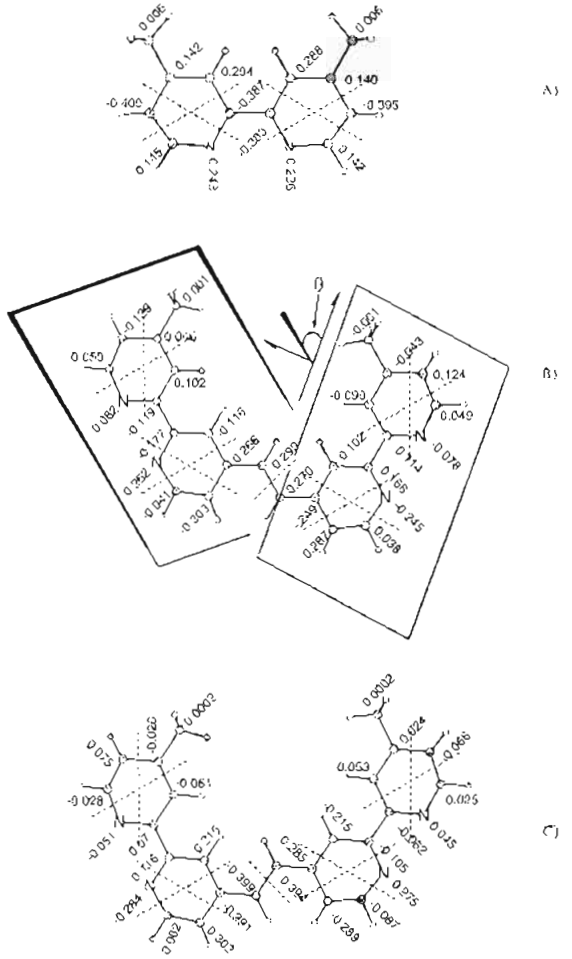

Figure 3. Results of AM$_1$ calculations for the LUMO of (A) dmb$^{\bullet-}$, (B) bbpe, (c) bbpe$^{\bullet-}$. θ is the angle defined by the bipyridyl planes. It is 22.7° in bbpe and 0° in bbpe$^{\bullet-}$. The numbers in the figure represent the p_z orbital coefficient in the molecular orbital and the dashed lines are calculated nodes.

buffered eluent which causes separation by charge differences. Typically, a 30 min gradient ramp was employed from 0 to 2 mM KBr. Elution of the Br^- salts was monitored at 300 and 480 nm on a variable UV−vis detector. Band retention times were proportional to the slope of the linear ramp, and varied with molecular charge. Isolation of the PF_6^- salts by metathases resulted in materials which were free of interfering impurities for photophysical studies.

Results

Synthesis and Characterization of 1,2-Bis(4-(4′-methyl)-2,2′-bipyridine)ethene. The synthetic strategy adopted for the preparation of bbpe (Figure 2) involved compounds **1** and **2** as synthetic intermediates. These compounds were prepared by partial oxidation of one of the methyl groups of dmb by either SeO_2[35] or NBS.[36-38] Formation of the triphenylphosphonium bromide salt by the reaction between **2** and a 10-fold excess of PPh_3 in toluene was nearly quantitative. The coupling of **1** and **3** via the Wittig reaction[38] proceeded in ca. 50% yield. The ^{1}H NMR spectrum of the product was consistent with the formation of a single isomer. From the unusually low-field resonance of the olefinic protons in the ^{1}H NMR (δ = 7.42 ppm), we infer that the *trans*-isomer is the sole product.[39]

We have been unable to detect a luminescence from bbpe in CH_2Cl_2 at room temperature. This is also the case for stilbene and its derivatives, where $\pi \rightarrow \pi^*$ excitation leads to a twisting about the olefinic bond, which provides a rapid nonradiative decay pathway.[40] A weak, structured fluorescence at 390 nm is detectable in 4:1 (v:v) EtOH−MeOH at 298 K upon 300 nm excitation. In the presence of added ethyl iodide ($\sim 1 \times 10^{-4}$ M) a weak, structured phosphorescence was observed with maxima at 600, 660, and 725 nm. Direct UV irradiation (1 h at 300 nm) produced no detectable changes in the electronic absorption or ^{1}H NMR spectra of bbpe. If a photoinduced *trans* → *cis* isomerization does occur, the ratio of *trans* to *cis* in the photostationary state must be >100:1.

In CH_2Cl_2 solutions containing bbpe at concentrations up to 1×10^{-2} M, no detectable quenching of emission from $[Ru(dmb)_3]^{2+}$ was observed. Stilbene and related derivatives are known to quench $[Ru(bpy)_3]^{2+*}$, suggesting that the energy of the lowest lying π-π^* excited state in the uncoordinated ligand is >2.1 eV.[41,42]

Retention of the trans-isomer of bbpe in the complexes was verified by the low field resonances for the −CH=CH− protons that appear in the ^{1}H NMR spectra. As for the pure ligand, no photoinduced isomerism of the ligand in the metal complexes occurred upon irradiation. This is not a surprising result. Molecular models indicate that the *cis*-configuration would bring the two dicationic complexes into very close proximity, a configuration which would be disfavored electrostatically.

AM1 Calculations. Molecular orbital calculations were carried out by using AM1 parameters for dmb and bbpe for both the neutral molecules and radical anions with the N atoms and bipyridyl ring systems parametrized as aromatic. From the full Cartesian gradient optimization of the ligand basis set, structural representations of the electronic levels can be calculated and represented as Cartesian coordinates.[32] The results for the lowest π^* orbitals of bbpe and bbpe$^{\bullet-}$ are illustrated in Figure 3. For comparison, the orbital eigenvectors are also included for the radical anion of DMB in Figure 3. The results of the calculations of bond length, bond angles, and twist angles are given in supplemental Tables 1−4. Calculations conducted with the N atoms protonated gave similar results for the N atom coefficients in the lowest π^* orbital level in both the neutral molecule and anion.

The molecular structure of bbpe (Figure 3A) is predicted by the AM1 calculation to exhibit a canting between the two planes defined by the bipyridyl rings. The canting angle is the dihedral angle (θ) formed by the 3-C's on the two rings and the double bond. It is 22.7° in bbpe and 0° in the radical anion. The molecular structure, p_z orbital contributions to the lowest π^* orbitals, and the calculated orbital nodes are also shown. Inspection of the orbital coefficients reveals an asymmetry in the ligand π-system due to the canting of the rings. There is a considerable asymmetry in the orbital coefficients for separate

(35) Rabjohn, N. *Org. React.* **1965**, *14*, 270.
(36) Eaves, J. G.; Munro, H. S.; Parker, D. *Inorg. Chem.* **1987**, *26*, 244.
(37) Lehn, J.-M.; Rigault, A.; Siegel, J.; Harrowfield, J.; Chevrier, B.; Moras, D. *Proc. Natl. Acad. Sci. U.S.A.* **1987**, *84*, 2565.
(38) Maercker, A. *Org. React.* **1965**, *14*, 270.
(39) Williams, D. H.; Fleming, I. *Spectroscopic Methods in Organic Chemistry*; McGraw-Hill: London, 1980.
(40) (a) Hammond, G. S.; Saltiel, J.; Camola, A. A.; Turro, N. J.; Bradshaw, J. S.; Cowan, D. O.; Counsell, R. C.; Vogt, V.; Dalton, C. *J. Am. Chem. Soc.* **1964**, *86*, 3197. (b) Malkin, S.; Fischer, E. *J. Phys. Chem.* **1964**, *68*, 1153.
(41) (a) Wrighton, M.; Markham, J. *J. Phys. Chem.* **1973**, *77*, 3042. (b) Hoffman, M. Z., Bolletta, F.; Moggi, L.; Hug, G. L. *J. Phys. Chem. Ref. Data*, **1989**, *18*, 219. (c) Whitten, *Acc. Chem. Res.* **1980**, *13*, 83.
(42) (a) Bock, C. R.; Connor, J. A.; Gutierrez, A. R.; Meyer, T. J.; Whitten, D. G.; Sullivan, B. P.; Nagle, J. K. *J. Am. Chem. Soc.* **1979**, *101*, 4815. (b) Toma, H. E.; Creutz, C. *Inorg. Chem.* **1977**, *16*, 545. (c) Ballardini, R.; Varani, G.; Indelli, M. T.; Scandola, F.; Balzani, V. *J. Am. Chem. Soc.* **1978**, *100*, 7219. (d) Rehm, D.; Weller, A. *Ber. Bunsen-Ges. Phys. Chem.* **1969**, *73*, 834. (e) Rehm, D.; Weller, A. *Isr. J. Chem.* **1970**, *8*, 259.

pyridyl rings of a bpy with the LUMO dominated by the rings directly linked to the olefin.

Electrochemistry. $E_{1/2}$ values for M(III/II) couples and ligand-based reductions in 0.1 M $[N(n\text{-}C_4H_9)_4](PF_6)$ in CH_3CN are listed in Table 1.

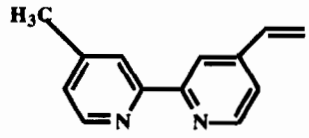

vbpy

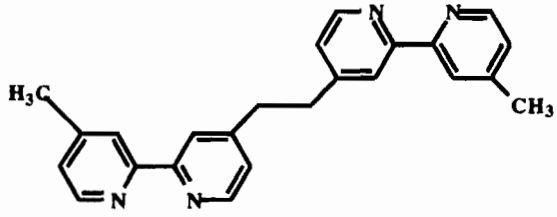

bbpa

For $[(dmb)_2Ru(\mu\text{-bbpe})Ru(dmb)_2]^{4+}$ and $[(bpy)_2 Os(\mu\text{-bbpe}) Os(bpy)_2]^{4+}$ only a single, unresolved wave (at 1.16 V for M = Ru and 0.80 V for M = Os) was observed for the M(III/II) couples. The peak-to-peak splittings, ΔE_p ($=E_{p,a} - E_{p,c}$) ~90 ± 5 mV, were larger than ΔE_p = 70 ± 5 mV for the one-electron couples of $[Ru(dmb)_3]^{3+/2+}$, $[Os(bpy)_3]^{3+/2+}$ or $[Ru(dmb)_2(bbpe)]^{3+/2+}$ and the integrated areas twice that of the one-electron couples. For the two-electron couple for $[(dmb)_2Ru(\mu\text{-bbpa})Ru(dmb)_2]^{4+}$, in which there is no orbital basis for significant electronic coupling, ΔE_p = 75 ± 5 mV, 70 ± 5 mV for $[(bpy)_2Os(\mu\text{-bbpa})Os(bpy)_2]^{4+}$.

Two, bbpe-based, one-electron waves appear, and at more negative potentials unresolved, two-electron reductions at bpy or dmp. Peak to peak separations for the two-electron waves were ~100 mV and the integrated peak areas twice those of the one-electron couples.

Electrolysis of the bridged complexes in 0.1 M $[N(n\text{-}C_4H_9)_4](PF_6)$ in CH_3CN at −1.1 V vs SSCE resulted in hydrogenation of the double bond. The UV−visible absorption spectrum at the end of the electrolysis was coincident with the spectrum of the bbpa complex. The spectra of the one-electron reduced complexes could be obtained in dry dimethoxyethane (DME). Spectroelectrochemical, one-electron reduction of $[(bpy)_2Os(\mu\text{-bbpe})Os(bpy)_2]^{4+}$ at −1.4 V versus a silver wire in 0.2 M $[N(C_4H_9)_4](ClO_4)$ in DME resulted in bands for $bbpe^{\bullet-}$ at 400, 610 (broad), and 780 nm (weak). One-electron reduction of the Ru complex in 0.2 M $LiClO_4$ in THF at −2.20 V vs a silver wire in an OTTL cell (under N_2) gave a new band at 495 nm and a weak, broad band at 700 nm (supplemental Figure 1).

Mixed-Valence Ions. Solutions the mixed-valence ions $[(dmb)_2 M (\mu\text{-bbpe}) M (dmb)_2]^{5+}$ (M = Ru, Os) were generated by electrochemical oxidation in 0.1 M $[N(n\text{-}C_4H_9)_4](PF_6)$ in CD_3CN at a Pt electrode to n = 1. For M = Ru the solutions were unstable toward spontaneous reduction of Ru^{III} to Ru^{II}. Solutions containing $Os^{III}-Os^{II}$ were also generated by mixing equimolar amounts of $Os^{III}-Os^{III}$ and $Os^{II}-Os^{II}$. The $Ru^{II}-Ru^{II}$ ion was stabilized in 1 N H_2SO_4 ($t_{1/2}$ = 83 min) following oxidation of $Ru^{III}-Ru^{II}$ by $[Ce(NH_4)_6](NO_3)$. Re-reduction of $Ru^{III}-Ru^{II}$ or $Os^{III}-Os^{II}$ by L-ascorbic acid gave back the $Ru^{II}-Ru^{II}$ or $Os^{II}-Os^{II}$ spectra quantitatively.

In the near-infrared (NIR) spectrum of $Os^{III}-Os^{II}$, broad intervalence transfer (IT) bands appear at λ_{max} ~910 and 1352 nm and $d\pi \rightarrow d\pi$ (Os^{III}) bands at 1990 (ϵ = 330 M^{-1} cm^{-1}) and 2100 nm (ϵ = 375 M^{-1} cm^{-1}). For $Ru^{III}-Ru^{II}$, a broad, weak IT band appears at ~1300 nm.

Comproportionation equilibrium constants, eq 9, of $K_c \sim 15$ (M = Ru, Os) were calculated by applying the global minimization routine described by Maeder and Zuberbühler to spectra changes accompanying Ce^{IV} titrations.[43] The spectra of the

$$M^{III}-M^{III} + M^{II}-M^{II} \overset{K_c}{\rightleftharpoons} 2M^{III}-M^{II} \quad (8)$$

$$K_c = \frac{[M^{III}-M^{II}]}{[M^{III}-M^{III}][M^{II}-M^{II}]} \quad (9)$$

$M^{III}-M^{II}$ ions were also obtained in the analyses, Figure 4. The values for K_c are consistent with K_c (μ = 0.1, 298 K) ~ 15 in CH_3CN calculated from the electrochemical data by the procedure of Richardson and Taube.[44] For $[(dmb)_2Ru(\mu\text{-bbpa})\text{-}Ru(dmb)_2]^{4+}$ in CH_3CN (0.1 M $[N(n\text{-}C_4H_9)_4](PF_6)$), $K_c \sim 8.5$ from the electrochemical analysis which is within a factor of 2 of the statistical value of 4 expected for a noninteracting system.[44] If electrostatic and statistical effects are comparable between the bbpe and bbpa complexes, electronic delocalization favors $Ru^{III}-Ru^{II}$ in the former by ~15 meV.

Incremental oxidation of $M^{II}-M^{II}$ (M = Ru, Os) by Ce^{IV} (10^{-6} M) in 1 N H_2SO_4 resulted in a linear decrease in emission intensity with no change in band shape. There was no evidence for emission from the mixed-valence ions as shown by the plots of I_{em} vs Ce^{IV} equivalents added, Figure 5. The dotted lines were calculated by assuming K_c = 15 and emission arising solely from $M^{II}-M^{II}$. The experimental points coincide with the calculated plot within experimental error.

Absorption and Emission Spectra and Excited State Properties. Absorption spectra are shown in Figure 6, and band assignments, in Table 1. Emission spectra for $[(dmb)_2Ru(\mu\text{-}bbpe)Ru(dmb)_2]^{4+}$ in 4:1 (v:v) ethanol−methanol at 77 and 298 K are shown in Figure 7 as are calculated spectra (eq 4) as dashed lines. The parameters used in the calculations are listed in Table 2. The weak emission at >15 000 cm^{-1} resembles $[Ru(dmb)_3]^{2+*}$ and is from a trace impurity not observable in the NMR. We assume it to be a Ru^{II} dimer with the olefinic group of bbpe hydroxylated or hydrogenated. The emission quantum yield for $[Ru(dmb)_3]^{2+*}$ is 20 times greater than for $[(dmb)_2Ru(\mu\text{-bbpe})Ru(dmb)_2]^{4+*}$, Table 3, and either of the proposed impurities would be relatively strong emitters as well. Emission quantum yields (ϕ_{em}) and maxima are given in Table 3. Excitation spectra overlay absorption spectra for $[(dmb)_2\text{-}M(\mu\text{-bbpe})M(dmb)_2]^{4+}$ (M = Ru, Os) monitored at 800 nm for M = Ru and at 850 nm for M = Os.

Emission lifetimes in CH_3CN at room temperature and in 4:1 (V:V) ethanol-methanol at 77 and 298K are listed in Table 3. Lifetime variations with temperature in the alcohol mixture are shown in Figure 8. Lifetimes were independent of monitoring (500 to 800 nm) or excitation wavelengths (420−460 nm). Radiative (k_r) and nonradiative (k_{nr}) decay rate constants calculated by eqs 10 and 11 are also listed in Table 3. In

$$\tau^{-1} = k_r + k_{nr} \quad (10)$$

$$\eta\phi_{em} = k_r\tau^{-1} \quad (11)$$

calculating k_r, it was assumed that η, the quantum efficiency for reaching the emitting state is 1. Upper limits for quantum yields for ligand loss (Φ_p) in 2 mM $[N(n\text{-}C_4H_9)_4]Cl$ in CH_3CN solutions are listed in Table 3.

Table 1. $E_{1/2}$ and Spectral Data For Ru(II) and Os(II) Complexes in CH_3CN[a]

complex	$E_{1/2}$ (V)[a] oxidation	$E_{1/2}$ (V)[a] reduction	λ_{max} (nm) ϵ (M^{-1} cm^{-1})[b]	assignment
$[Ru(dmb)_3]^{2+}$	+1.13	−1.45	288 (73100)	$\pi \rightarrow \pi^*$(dmb)
		−1.64	328 (9950)	$d\pi \rightarrow \pi^*$(dmb)
		−1.88	360 (6040)	$d\pi \rightarrow \pi^*$(dmb)
			432 (10500)	$d\pi \rightarrow \pi^*$(dmb)
			458 (12650)	$d\pi \rightarrow \pi^*$(dmb)
$[Ru(dmb)_2(vbpy)]^{2+}$	+1.14	−1.36	288 (75200)	$\pi \rightarrow \pi^*$(dmb, vbpy)
		−1.60	332 (13200)	$d\pi \rightarrow \pi^*$(dmb, vbpy)
		−1.83	440 (15580)	$d\pi \rightarrow \pi^*$(dmb, vbpy)
			464 (17400)	$d\pi \rightarrow \pi^*$(dmb, vbpy)
$[(dmb)_2Ru(\mu\text{-bbpe})(Ru(dmb)_2]^{4+}$	+1.16	−1.07	288 (80610)	$\pi \rightarrow \pi^*$(dmb, bbpe)
		−1.33	335 (sh)	$d\pi \rightarrow \pi^*$(dmb, bbpe)
		−1.65	460 (22250)	$d\pi \rightarrow \pi^*$(dmb, bbpe)
			500 (25810)	$d\pi \rightarrow \pi^*$(bbpe)
$[(dmb)_2Ru(bbpe)]^{2+}$	+1.15	−1.04	290 (69000)	$\pi \rightarrow \pi^*$(dmb, bbpe)
		−1.30	315 (sh)	$d\pi \rightarrow \pi^*$(dmb, bbpe)
		−1.65	335 (sh)	$d\pi \rightarrow \pi^*$(dmb, bbpe)
			482 (20300)	$d\pi \rightarrow \pi^*$(dmb, bbpe)
$[(dmb)_2Ru(\mu\text{-bbpa})(Ru(dmb)_2]^{4+}$	+1.11	−1.43	288 (120000)	$\pi \rightarrow \pi^*$(dmb, bbpa)
		−1.65	330 (sh)	$d\pi \rightarrow \pi^*$(dmb, bbpa)
		−1.87	360 (sh)	$d\pi \rightarrow \pi^*$(dmb, bbpa)
			436 (22200)	$d\pi \rightarrow \pi^*$(dmb, bbpa)
			464 (25400)	$d\pi \rightarrow \pi^*$(dmb, bbpa)
$[Os(dmb)_3]^{2+}$	+0.68	−1.38	292 (64660)	$\pi \rightarrow \pi^*$(dmb)
		−1.56	336 (9200)	$d\pi \rightarrow \pi^*$(dmb)
		−1.86	380 (9460)	$d\pi \rightarrow \pi^*$(dmb)
			460 (10225)	$d\pi \rightarrow \pi^*$(dmb)
			488 (10325)	$d\pi \rightarrow \pi^*$(dmb)
			658 (2820)	$d\pi \rightarrow \pi^*$(dmb)
$[Os(bpy)_3]^{2+}$	+0.84	−1.26	290 (79360)	$\pi \rightarrow \pi^*$(bpy)
		−1.46	328 (8860)	$d\pi \rightarrow \pi^*$(bpy)
		−1.78	370 (9130)	$d\pi \rightarrow \pi^*$(bpy)
			386 (8880)	$d\pi \rightarrow \pi^*$(bpy)
			446 (11490)	$d\pi \rightarrow \pi^*$(bpy)
			480 (12110)	$d\pi \rightarrow \pi^*$(bpy)
			658 (2760)	$d\pi \rightarrow \pi^*$(bpy)
$[(bpy)_2Os(\mu\text{-bbpe})Os(bpy)_2]^{4+}$	+0.80	−1.07	292 (84900)	$\pi \rightarrow \pi^*$(bpy, bbpe)
		−1.22	460 (19100)	$d\pi \rightarrow \pi^*$(bpy, bbpe)
		−1.60	516 (24200)	$d\pi \rightarrow \pi^*$(bbpe)
			682 (8520)	$d\pi \rightarrow \pi^*$(bpy, bbpe)
$[(bpy)_2Os(bbpe)]^{2+}$	+0.80	−1.07	292 (75000)	$\pi \rightarrow \pi^*$(bpy, bbpe)
		−1.22	392 (sh)	$d\pi \rightarrow \pi^*$(bpy, bbpe)
		−1.60	458 (14970)	$d\pi \rightarrow \pi^*$(bpy, bbpe)
			494 (16980)	$d\pi \rightarrow \pi^*$(bbpe)
			668 (4670)	$d\pi \rightarrow \pi^*$(bpy, bbpe)
$[(bpy)_2Os(\mu\text{-bbpa})Os(bpy)_2]^{4+}$	+0.78	−1.39	290 (72350)	$\pi \rightarrow \pi^*$(bpy, bbpa)
		−1.51	330 (12000)	$d\pi \rightarrow \pi^*$(bpy, bbpa)
		−1.85	372 (12500)	$d\pi \rightarrow \pi^*$(bpy, bbpa)
			452 (14400)	$d\pi \rightarrow \pi^*$(bpy, bbpa)
			484 (14850)	$d\pi \rightarrow \pi^*$(bpy, bbpa)
			652 (3800)	$d\pi \rightarrow \pi^*$(bpy, bbpa)

[a] From cyclic voltammetric measurements on 0.1 M $[N(n\text{-}C_4H_9)_4](PF_6)$ in CH_3CN solutions vs SSCE at a 1 cm Pt disk electrode at 100 mV/s; $E_{1/2}$ = 0.307 V for the $Fe(C_5H_5)_2^{+/0}$ couple under these conditions. [b] From measurements on solutions in the range 1×10^{-6} to 6×10^{-6} M.

Transient absorption difference spectra in CH_3CN are shown in Figure 9. Those for $[Ru(dmb)_3]^{2+}$, $[Os(dmb)_3]^{2+}$, and $[Ru(dmb)_2(vbpy)]^{2+}$ are included as supplemental data (supplemental Figure 2). The transient absorption spectra decayed with the same lifetimes as emission.

In an attempt to discern absorption features in the excited state, calculated spectra, $A^*(\lambda)$, were generated by adding the ground state spectra to transient difference spectra, supplemental Figure 3. The simulations were generated by adding fractional amounts of the ground state spectrum, $A(\lambda)$, to the difference spectrum, $\Delta A(\lambda)$, eq 12, and allowing b to vary from 0 to 1. The isosbestic points were arbitrarily set to 0 absorbance units.

$$\Delta A^*(\lambda) = (1 - b)\Delta A(\lambda) + bA(\lambda) \qquad (12)$$

Features that appeared for $[(dmb)_2Ru(\mu\text{-bbpe})Ru(dmb)_2]^{4+*}$ by using this procedure were a broad $\pi^* \rightarrow \pi^*$ band near 585 nm, a lower energy $\pi^* \rightarrow \pi^*$ band at ~700 nm, $d\pi(Ru^{II}) \rightarrow \pi^*$(dmb, bbpe) bands at 460 and 515 nm, and $\pi \rightarrow \pi^*$ bands at 360 and 395 nm. For $[(bpy)_2Os(\mu\text{-bbpe})Os(bpy)_2]^{4+*}$, $d\pi(Os^{II}) \rightarrow \pi^*$(bpy, bbpe) bands appeared at 460 and ~520 nm,

(43) (a) Maeder, M.; Zuberbühler, A. D. *Anal. Chem.* **1990**, *62*, 2220. (b) Ozeki, T.; Kihara, H.; Ikeda, S. *Anal. Chem.* **1988**, *60*, 2055. (c) Gampp, H.; Maeder, M.; Meyer, C. J.; Zuberbühler, A. D. *Talanta* **1986**, *33*, 943. (d) The program SPECFIT, described by Maeder, was modified to perform kinetic analyses by Dr. R. A. Binstead.
(44) Richardson, D. E.; Taube, H. *Inorg. Chem.* **1981**, *20*, 1278.

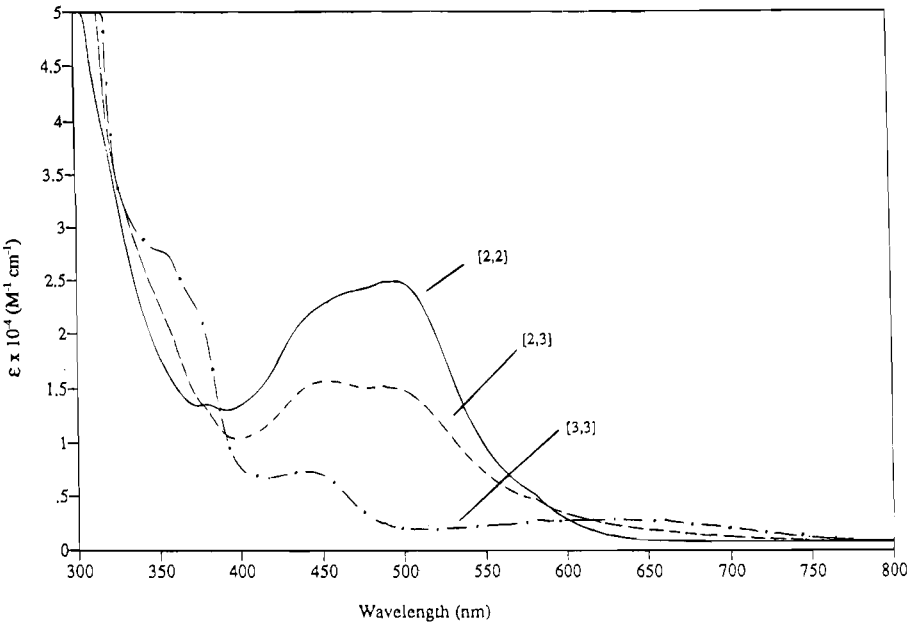

Figure 4. Calculated spectra for the [2,2] (—), [2,3] (- -), and [3,3] (— • —) forms of $[(dmb)_2Ru(\mu\text{-bbpe})Ru(dmb)_2](PF_6)_4$ in 1 N H_2SO_4 generated by global analysis of data obtained in the Ce^{IV} titration of $M^{II}-M^{II}$ to $M^{III}-M^{III}$.

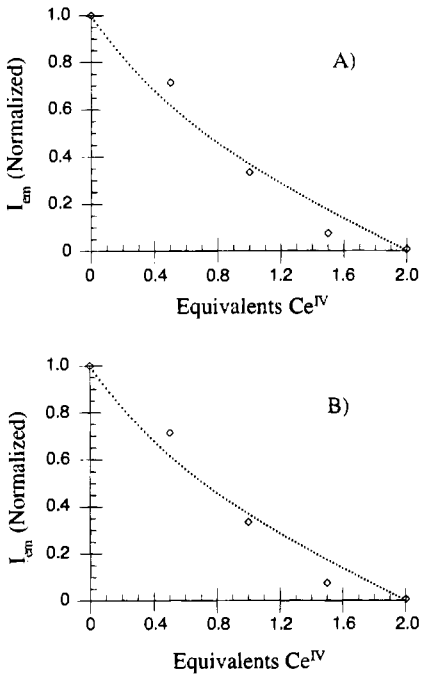

Figure 5. Plot of the relative emission intensity (I_{em}) vs added Ce^{IV} (◇) in 1*N* H_2SO_4 and the value I_{em} calculated by assuming that emission comes solely from $M^{II}-M^{II}$ by using eq 10, and $K_c = 15$ (dotted line) for (a) $[(dmb)_2Ru(\mu\text{-bbpe})Ru(dmb)_2](PF_6)_4$ and (b) $[(bpy)_2Os(\mu\text{-bbpe})Os(bpy)_2](PF_6)_4$.

an intense $\pi^* \rightarrow \pi^*$ band at 580 nm, a weaker $\pi^* \rightarrow \pi^*$ band at >650 nm, and additional $\pi \rightarrow \pi^*$ bands at 380 and 400 nm.

Ground and Excited State Resonance Raman. In Table 4 are listed energies of Raman bands that were resonantly enhanced following MLCT excitation of CH_3CN solutions 1×10^{-3} M in $[(dmb)_2Ru(\mu\text{-bbpe})Ru(dmb)_2](PF_6)_4$ or $[(bpy)_2Os(\mu\text{-bbpe})Os(bpy)_2](PF_6)_4$ and, for comparison, $[Ru(dmb)_3](PF_6)_2$ and $[Os(bpy)_3](PF_6)_2$. Assignments of bands at 1186, 1215, 1330, 1425, 1531, and 1638 cm^{-1} to bbpe modes were based on the result of excitation dependence studies which show greater enhancements with 548.8 nm excitation where $M^{II} \rightarrow$ bbpe bands dominate the absorption spectra (Figure 6) compared to 457.9 nm. The band at 1638 cm^{-1} arises from the −C=C− stretch of the olefinic bridge, and the band at 1186 cm^{-1} from the C(ring)−C(olefin) stretch.[18a,45]

Excited (354.7 nm excitation and scattering) and ground state (488.0 nm) spectra of $[(dmb)_2Ru(\mu\text{-bbpe})Ru(dmb)_2](PF_6)_4$ in CH_3CN are shown in Figure 10. The Raman band energies are listed in Table 5 for the Os and Ru excited states and for $bbpe^{\bullet-}$ generated electrochemically in 0.1 M $LiClO_4$ in THF. There is a good correlation between many of the bands for $bbpe^{\bullet-}$ and the excited states and no bands for $dmb^{\bullet-}$ or $bpy^{\bullet-}$.[14,15,46] The spectra are complicated by what appear to be ground state bands for bpy or dmb.

In comparing the ground- and excited-state spectra for the Ru complex in Tables 4 and 5, the band at 1638 cm^{-1} is lost in the excited state and new bands appear at 1578 and 1585 cm^{-1}. (This change is somewhat obscured in the Os complex because of the presence of the intense band assigned to a ground-state bpy mode at 1606 cm^{-1}. The corresponding band for dmb is at 1618 cm^{-1}). In *trans*-stilbene the C=C stretch of the olefin bridge at 1638 cm^{-1} shifts to 1578 cm^{-1} in the radical anion and to 1586 cm^{-1} in the lowest lying triplet.[18a,47] By comparison, the 1638 cm^{-1} ground state band in the bbpe-bridged complexes can be assigned to the −C=C− stretch of the olefin bridge. It shifts to 1578 or 1585 cm^{-1} in the excited state and to 1575 cm^{-1} in $bbpe^{\bullet-}$ (Table 5). The other band of the pair at 1578 and 1585 cm^{-1} in $[(dmb)_2Ru(\mu\text{-bbpe})Ru(dmb)_2]^{4+*}$ is the ground state bbpe band at 1609 cm^{-1} shifted to lower energy in the excited state. In bpy and related ligands, this is predominantly a C=C ring stretching vibration.[15]

In the trans-stilbene radical anion, the C(ring)−C(olefin) stretch shifts to 1251 cm^{-1} from 1188 cm^{-1}. The shift is from 1186 to 1255 cm^{-1} in the bbpe excited states. Where correlations are possible, an average shift of ±10−20 cm^{-1} is observed for the ring modes in $[(dmb)_2Ru(\mu\text{-bbpe})Ru(dmb)_2]^{4+}$ between

(45) (a) Barker, D. J.; Cooney, R. P.; Summers, L. A. *J. Raman Spectrosc.* **1987**, *18*, 443. (b) Kihara, H.; Gondo, Y. *J. Raman Spectrsc.* **1986**, *17*, 263. (c) Yamagushi, S.; Yoshizumi, J.; Maeda, S. *J. Phys. Chem.* **1978**, *82*, 1078. (d) Forster, M.; Hester, R. E. *Chem. Phys. Lett.* **1981**, *101*, 42. (e) Hester, R. E.; Suzuki, S. *J. Phys. Chem.* **1982**, *86*, 4626.
(46) Bradley, P. G.; Hornberger, B. A.; Dallinger, R. F.; Woodruff, W. H. *J. Am. Chem. Soc.* **1981**, *103*, 7441.
(47) Langkilde, F. W.; Wilbrandt, R.; Negri, F.; Orlandi, G. *Chem. Phys. Lett.* **1990**, *165*, 66.

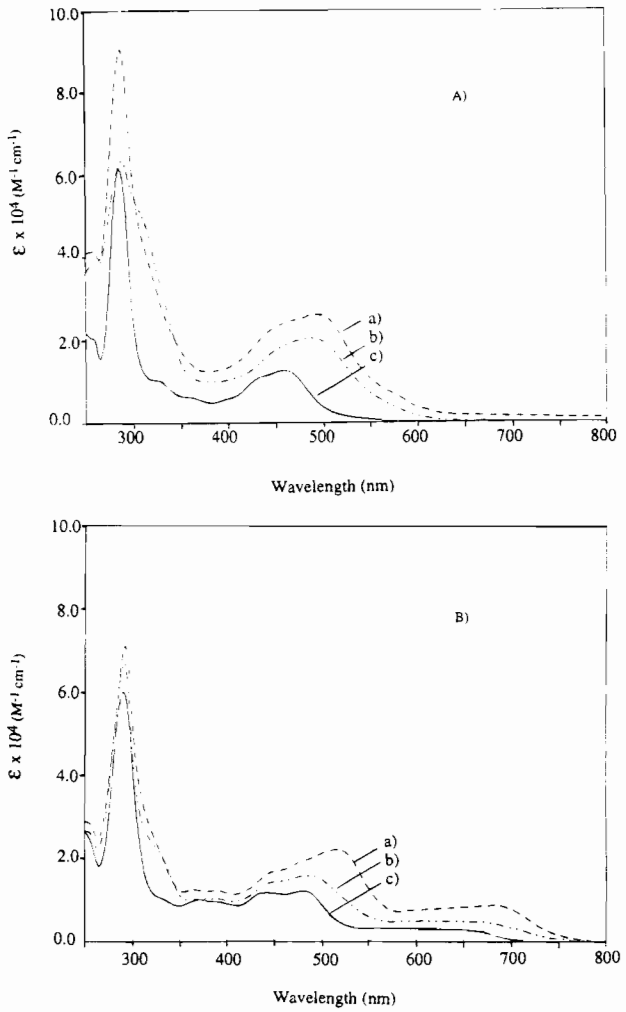

Figure 6. (A) Absorption spectra in CH_3CN at 298 K for (a) $[(dmb)_2Ru(\mu\text{-bbpe})Ru(dmb)_2](PF_6)_4$ (- -), (b) $[Ru(dmb)_2(bbpe)](PF_6)_2$ (— • • —), and (c) $[Ru(dmb)_3](PF_6)_2$ (—). (B) Absorption spectra in CH_3CN at 298 K for (a) $[((bpy)_2Os)_2(\mu\text{-bbpe})](PF_6)_4$ (- -), (b) $[((bpy)_2Os)(bbpe)](PF_6)_2$ (— • • —), and (c) $[Os(dmb)_3](PF_6)_2$ (—).

ground and excited state. For $[Ru(bpy)_3]^{2+}$, the shifts are 40–60 cm^{-1}.[13b,14a–c,15,46]

Discussion

The lowest energy excited states in $[(dmb)_2Ru(\mu\text{-bbpe})Ru(dmb)_2](PF_6)_4$ or $[(bpy)_2Os(\mu\text{-bbpe})Os(bpy)_2]^{4+}$ are bbpe-based MLCT states and not $\pi\pi^*$ as found in $[(dmb)_2Ru(dstyb)Ru(dmb)_2](PF_6)_4$.[48] The acceptor ligand is bbpe as shown by the common pattern of resonantly enhanced vibrations in the excited

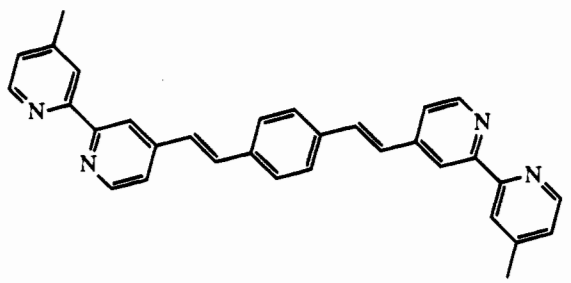

dstyb

states with $bbpe^{\bullet-}$. The shift in the −C=C− (olefin) stretch between ground and excited states in $[(dmb)_2Ru(\mu\text{-bbpe})Ru(dmb)_2](PF_6)_4$, is $\Delta\bar{\nu} \sim -50$ cm^{-1}. It is -59 cm^{-1} between *trans*-stilbene and its radical anion and -70 cm^{-1} for its triplet excited state.[18a,47] These complexes exhibit broad, structureless emissions at room temperature, typical MLCT vibronic structure at 77 K, Figure 7, temperature dependent lifetimes consistent with related MLCT emitters, Figure 8, and exponential decays.[49,50] The weak, structured phosphorescence from ^{3}bbpe at 600 nm in 4:1 (v:v) EtOH–MeOH is higher in energy by ~3300 cm^{-1} than the emitting MLCT state.

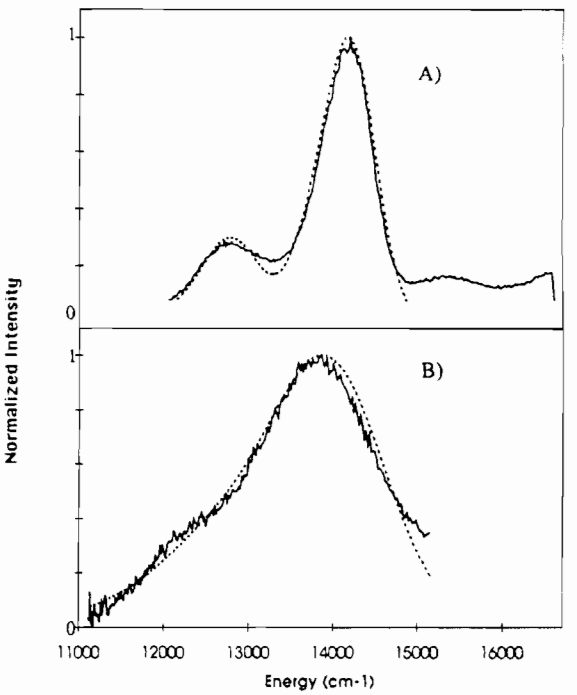

Figure 7. Emission spectra and fits of the spectra (dashed line) by using eqs 4–6 and the spectral fitting parameters in Table 3 for $[(dmb)_2Ru)(\mu\text{-bbpe})Ru(dmb)_2]^{4+}$ in 4:1 (v:v) ethanol–methanol at (A) 77 K and (B) 298 K. The weak emission at >15 000 cm^{-1} arises from an impurity, which is less than 0.1% of the total emission, as discussed in the text.

Mixed-Valence Properties. Electronic coupling between the metals in $[(dmb)_2Ru^{II}(\mu\text{-bbpe})Ru^{III}(dmb)_2]^{5+}$ and $[(bpy)_2Os^{II}(\mu\text{-bbpe})Os^{III}(bpy)_2]^{5+}$ is weak with a delocalization energy of ~15 meV based on the electrochemical measurements. Ru, Os → bbpe excitation of the M^{II}–M^{II} ions leads to an excited state

$$[(b)_2M^{II}(\mu\text{-bbpe})M^{II}(b)_2]^{4+} \xrightarrow{h\nu} [(b)_2M^{III}(\mu\text{-bbpe}^{\bullet-})M^{II}(b)_2]^{4+*} \quad (13)$$

mixed-valency, for which there are several possible limiting descriptions:

(1) The excited electron is delocalized over both bpy's in bbpe and the hole is delocalized as well—$[(b)_2M^{II.5}(\mu\text{-bbpe}^{\bullet-})M^{II.5}(b)_2]^{4+*}$.

(2) The hole is delocalized, but the electron is localized on one of the bpy's giving a pair of degenerate isomers—

(48) Shaw, J. R.; Webb, R. T.; Schmehl, R. H. *J. Am. Chem. Soc.* **1990**, *112*, 1117.

(49) (a) Lumpkin, R. S.; Kober, E. M.; Worl, L. A.; Murtaza, Z.; Meyer, T. J. *J. Phys. Chem.* **1990**, *94*, 239. (b) Danielson, E.; Lumpkin, R. D.; Meyer, T. J. *J. Phys. Chem.* **1987**, *91*, 1305.

(50) (a) Juris, A.; Barigelletti, F.; Balzani, V.; Belser, P.; Von Zelewsky, A. *Inorg. Chem.* **1985**, *24*, 202. (b) Barigelletti, F.; Juris, A.; Balzani, V.; Belser, P.; Von Zelewsky, A. *Inorg. Chem.* **1983**, *22*, 3335. (c) Wallace, W. M.; Hoggard, P. E. *Inorg. Chem.* **1980**, *19*, 2141. (d) Allsopp, S. R.; Cox, A.; Kemp, T. J.; Reed, W. J.; Carassiti, V.; Traverso, O. *J. Chem. Soc., Faraday Trans.* **1979**, *75*, 353. (e) Allsopp, S. R.; Cox, A.; Jenkins, S. H.; Kemp, T. J.; Tunstal, S. M. *Chem. Phys. Lett.* **1976**, *43*, 135. (f) Hager, C. D.; Crosby, G. A. *J. Am. Chem. Soc.* **1975**, *97*, 7031.

Table 2. Emission Spectral Fitting Parameters in 4:1 (v:v) Ethanol–Methanol[a]

salt	T (K)	E_{00} (cm^{-1})	$h\omega_M$ (cm^{-1})	S_M	$h\omega_L$ (cm^{-1})	S_L	$\Delta\bar{\nu}_{1/2}$ (cm^{-1})
$[Ru(dmb)_3](PF_6)_2$	77	17 250	1400	0.99	350	2.1	450
	298	16 350	1400	0.38	350	2.1	1900
$[Ru(dmb)_2(vbpy)](PF_6)_2$	77	17 050	1400	0.81	400	2.3	550
	298	16 000	1400	0.35	400	2.3	1500
$[(dmb)_2Ru(\mu\text{-bbpe})Ru(dmb)_2](PF_6)_4$	77	14 200	1400	0.40	400	0.34	700
	298	14 000	1400	0.38	400	0.34	1500
	157	14 000	1400	0.39	400	0.34	800
$[(Ru(dmb)_2)(bbpe)](PF_6)_2$	77	15 400	1350	0.75	400	1.5	675
	298	14 700	1350	0.45	400	1.5	1660
$[Ru(bpy)_2(py)(Cl)](PF_6)$	157	13 800	1350	0.72	400	1.8	1050

[a] By using eq 4–7. The experimental and calculated spectra are shown in Figure 7. The estimated uncertainties are $E_{00} \pm 5\%$, $h\omega_M \pm 5\%$, $S_M \pm 5\%$, $h\omega_L \pm 15\%$, $S_L \pm 15\%$, and $\Delta\bar{\nu}_{1/2} \pm 10\%$.

Table 3. Excited State Properties[a]

salt	solvent	T (±2K)	λ_{max}^{em} (±2 nm)	τ (±3% ns)	ϕ_{em} (±10%)	$k \times 10^{-5}$ (±3%)	$k_r \times 10^{-5}$ [b] (±5% s^{-1})	$k_{nr} \times 10^{-5}$ [b] (±5% s^{-1})	ϕ_p[c] (±5%)
$[Ru(dmb)_3](PF_6)_2$	CH_3CN	298	642	950	0.100	10.5	1.05	9.48	0.005
	E–M	77	625	4300		2.33			
	E–M	298	597	878	0.072	11.4	0.82	10.6	
$[Ru(dmb)_2(vbpy)](PF_6)_2$	CH_3CN	298	670	1350	0.076	7.41	0.56	6.85	
	E–M	77	658	5790		1.73			
	E–M	298	615	1380	0.130	7.25	0.94	6.31	
$[(dmb)_2Ru(\mu\text{-bbpe})Ru(dmb)_2](PF_6)_4$	CH_3CN	298	750	1310	0.005	7.63	0.04	7.59	<0.001
	E–M	77	710	4400		2.27			
	E–M	298	730	1500	0.008	6.67	0.05	6.62	
$[Ru(dmb)_2(bbpe)](PF_6)_4$	CH_3CN	298	732	1150	0.010	8.69	0.09	8.60	<0.001
$[Os(dmb)_3](PF_6)_2$	CH_3CN	298	764	33	0.004	303	1.2	302	<0.001
	E–M	77	730	640					
	E–M	298	755	37	0.001	285	3.0	284	
$[Os(bpy)_3](PF_6)_2$	CH_3CN	298	746	60	0.005	167	8.0	166	<0.001
$[(bpy)_2Os(\mu\text{-bbpe})Os(bpy)_2](PF_6)_4$	CH_3CN	298	>850	52					<0.001
	E–M	77	>850						
	E–M	298	>850	37					
$[Os(bpy)_2(bbpe)](PF_6)_2$	CH_3CN	298	810	58					<0.001

[a] The various terms are defined in the text. E–M is an abbreviation for the 4:1 (v:v) ethanol–methanol solvent mixture. [b] The radiative (k_r) and nonradiative (k_{nr}) rate constants were calculated by using eqs 10 and 11, see text. [c] Quantum yield for ligand loss in 0.2 M $N[n\text{-}(C_4H_9)_4](Cl)$–$CH_3CN$.

$[(b)_2M^{II.5}(^{\bullet-}bpy\text{-}CH{=}CH\text{-}bpy)M^{II.5}(b)_2]^{4+*}$, $(b)_2M^{II.5}(bpy\text{-}CH{=}CH\text{-}bpy^{\bullet-})M^{II.5}(b)_2]^{4+*}$.

(3) The hole is localized and the electron delocalized—$[(b)_2M^{III}(\mu\text{-}bbpe^{\bullet-})M^{II}(b)_2]^{4+*}$ and $[(b)_2M^{II}(\mu\text{-}bbpe^{\bullet-})M^{III}(b)_2]^{4+*}$. (This was assumed in eq 13.)

(4) Both the hole and electron are localized giving a pair of low energy isomers—$[(b)_2M^{III}(^{\bullet-}bpy\text{-}CH{=}CH\text{-}bpy)M^{II}(b)_2]^{4+*}$, $[(b)_2M^{II}(bpy\text{-}CH{=}CH\text{-}bpy^{\bullet-})M^{III}(b)_2]^{4+*}$—and a pair of high energy isomers—$[(b)_2M^{II}(^{\bullet-}bpy\text{-}CH{=}CH\text{-}bpy)M^{III}(b)_2]^{4+*}$, $[(b)_2M^{III}(bpy\text{-}CH{=}CH\text{-}bpy^{\bullet-})M^{II}(b)_2]^{4+*}$.

The excited electron appears to be delocalized across the olefin to a significant degree (cases 1 and 3) based on the shifts in the −C=C− (olefin) and C(ring)-C(olefin) vibrations relative to *trans*-stilbene$^{0/-}$. These shifts imply a decreased bond order at the olefin, an increased bond order between the bpy's and the olefin, and a LUMO in which the excited electron is delocalized to some degree over both bpy's.

Delocalization is consistent with the appearance of bands at 370 and ~640 nm in the simulated excited state spectrum for M = Ru (supplemental Figure 3). Related features have been found in singly reduced 4,4′-bipyridine or bipyridinium cations,[51] reduced stilbene,[18,19] complexes containing 4,4′-bipyridyl type ligands in which the electron is thought to be delocalized over both pyridyl rings,[52–54] and in the excited states of complexes such as $[(bpy)_2(CO)Os^{II}(4,4'\text{-}bpy)Os^{II}(Cl)(phen)(cis\text{-}Ph_2PCH{=}CHPPh_2)]^{3+}$ (phen is 1,10-phenanthroline) or $[(bpy)Re(CO)_3(MQ^+)]^{2+}$, in which the excited electron is delocalized over both rings of the acceptor ligand.[53] There is also some

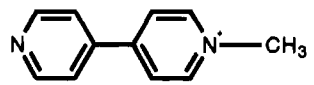

(MQ+)

evidence in the spectra for localization at the metals (case 3) from the appearance of bands assignable to $d\pi \rightarrow \pi^*$(dmb,bbpe) transitions at ~450, ~490, and perhaps ~540 nm for $[(dmb)_2Ru(\mu\text{-bbpe})Ru(dmb)_2]^{4+*}$. Case 3 would also explain the apparent ground state dmb/bpy enhancements in the excited state Raman data in Table 5. This would occur though resonance enhancement of bpy/dmb modes via scattering off high energy $d\pi(Ru^{II}) \rightarrow \pi^*$(bpy,dmb) transitions, Table 1.

(51) (a) Watanabe, T.; Honda, K. *J. Phys. Chem.* **1982**, *86*, 2617. (b) Kosower, E. M.; Cotter, J. L. *J. Am. Chem. Soc.* **1984**, *86*, 5524.

(52) (a) Tapolsky, G.; Duesing, R.; Meyer, T. J. *J. Phys. Chem.* **1989**, *93*, 3885. (b) Tapolsky, G.; Duesing, R.; Meyer, T. J. *Inorg. Chem.* **1990**, *29*, 2293.

(53) Chen, P.; Curry, M.; Meyer, T. J. *Inorg. Chem.* **1989**, *28*, 2272.

(54) (a) Chen, P.; Danielson, E.; Meyer, T. J. *J. Phys. Chem.* **1988**, *92*, 3708. (b) Chen, P.; Westmoreland, T. D.; Danielson, E.; Schanze, K. S.; Anthon, D., Neveux, P. E.; Meyer, T. J. *Inorg. Chem.* **1987**, *26*, 1116.

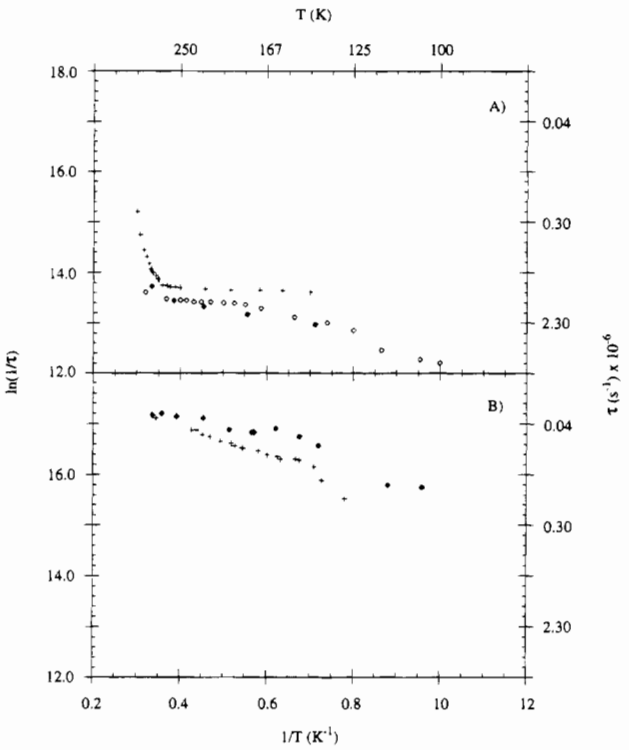

Figure 8. Variations in lifetime with temperature in 4:1 (v:v) ethanol–methanol for (A) $[Ru(dmb)_3](PF_6)_2$ (+++), $[Ru(bpy)_2(vbpy)](PF_6)_2$ (◇◇◇), and $[(dmb)_2Ru(\mu\text{-bbpe})Ru(dmb)_2](PF_6)_4$ (◆◆◆) and for (B) $[Os(dmb)_3(PF_6)_2$ (+++) and $[(bpy)_2Os(\mu\text{-bbpe})Os(bpy)_2](PF_6)_2$ (◆◆◆).

Although somewhat delocalized over both bpy's, the excited electron is necessarily asymmetrically distributed in the π^* acceptor orbital if there are separate Ru^{II} and Ru^{III} sites in the excited state.

We were unable to obtain evidence for transient intermediates following MLCT excitation of $[(dmb)_2Ru^{III}(\mu\text{-bbpe})Ru^{II}(dmb)_2]^{5+}$ or $[(bpy)_2Os^{III}(\mu\text{-bbpe})Os^{II}(bpy)_2]^{5+}$. Our interest in these excited states arose, in part, from the implied symmetrical nature of the excited state formed following MLCT excitation. Their lifetimes are <10 ns.

$$[(bpy)_2Os^{II}(\mu\text{-bbpe})Os^{III}(bpy)_2]^{5+} \xrightarrow{h\nu} [(bpy)_2Os^{III}(\mu\text{-bbpe}^{\bullet-})Os^{III}(bpy)_2]^{5+*}$$

dd States. From the coincidence between excitation and absorption spectra for $[(dmb)_2Ru(\mu\text{-bbpe})Ru(dmb)_2]^{4+}$ and $[(bpy)_2Os(\mu\text{-bbpe})Os(bpy)_2]^{4+}$, excitation from 350 to 600 nm gives bbpe-based MLCT states with equal efficiency either by direct $d\pi \rightarrow \pi^*$(bbpe) excitation or by internal sensitization following higher energy $d\pi \rightarrow \pi^*$(dmb,bpy) excitation.

In contrast to $[Ru(bpy)_3]^{2+}$ and $[Ru(dmb)_3]^{2+}$ (Table 3), $[(dmb)_2Ru(\mu\text{-bbpe})Ru(dmb)_2]^{4+}$ is photochemically inert toward ligand loss.[1,55] Photochemical instability in these complexes is thought to arise from MLCT excitation followed by thermally activated crossing to lowlying dd states which undergo ligand loss. The temperature dependence of τ for $[Ru(dmb)_3]^{2+}$ in Figure 8 is more-or-less typical of dd state involvement in the excited state manifold. Variation with T is negligible from the glass-to-fluid transition at 130–140 K to the onset of significant dd state population at 250 K.[50,55] There is no evidence for this behavior in $[(dmb)_2Ru(\mu\text{-bbpe})Ru(dmb)_2]^{4+}$ or $[Ru(dmb)_2(vbpy)]^{2+}$. The temperature dependences are complicated (perhaps as a consequence of the low symmetry), but there is no evidence for dd state involvement. This is understandable qualitatively. Compared to $[Ru(dmb)_3]^{2+}$, the lower lying π^* acceptor orbital at bbpe decreases the energy of the lowest MLCT state by >2000 cm^{-1}.

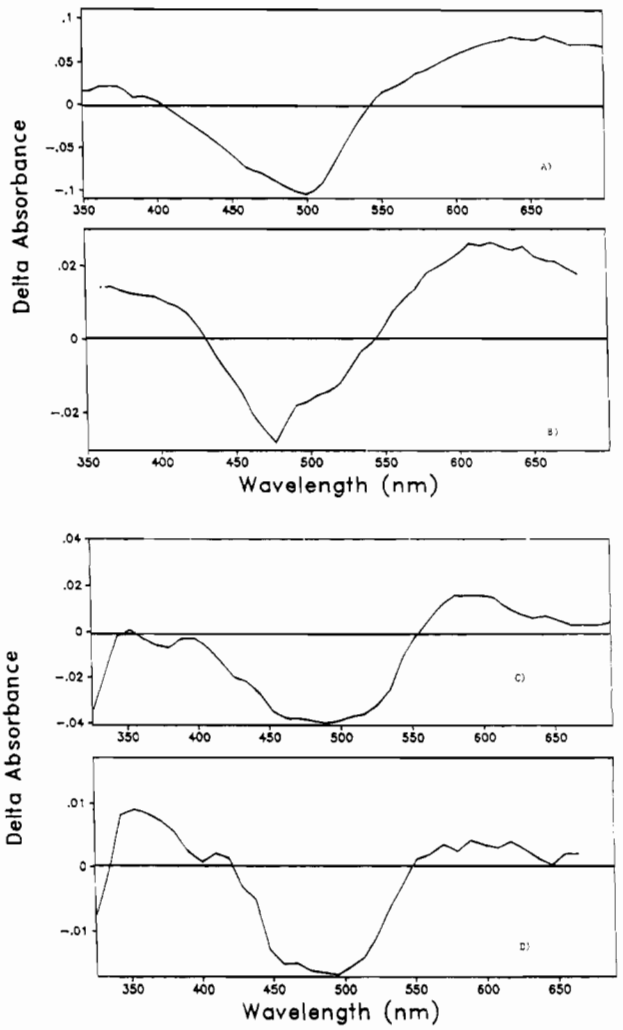

Figure 9. Transient absorption difference spectra acquired 80 ns after 5 μJ pulse excitation at 460 nm in CH_3CN solutions 1×10^{-5} M: (A) $[(dmb)_2Ru(\mu\text{-bbpe})Ru(dmb)_2]^{4+}$; (B) $[(dmb)_2Ru(bbpe)]^{2+}$, (C) $[(bpy)_2Os(\mu\text{-bbpe})Os(bpy)_2]^{4+}$; (D) $[(bpy)_2Os(bbpe)]^{2+}$.

Nonradiative Decay. Lifetimes for the bbpe complexes in Table 3 are remarkably long given the low excited state energies. In order to quantitate the effect it is necessary to make comparisons between complexes having comparable energy gaps and the same electronic origin. The comparison between $[(dmb)_2Ru(\mu\text{-bbpe})Ru(dmb)_2]^{4+*}$ (E_{00} = 14 000 cm^{-1}) and $[Ru(bpy)_2(py)Cl]^{+*}$ (E_{00} = 13 800 cm^{-1}) at 157 K in 4:1 (v:v) EtOH–MeOH is free of interference from higher lying states. At this temperature there is no complication of thermal population of higher lying MLCT or dd states. At 157 K τ = 104 ± 10 ns ($k_{nr} = 9.6 \times 10^6$ s^{-1}) for $[Ru(bpy)_2(py)Cl]^{+*}$ and 1.97 ± 0.05 μs ($k_{nr} = 6.6 \times 10^5$ s^{-1}) for $[(dmb)_2Ru(\mu\text{-bbpe})Ru(dmb)_2]^{4+*}$. $[Ru(dmb)_2(bbpe)]^{2+*}$ is long-lived as well (Table 3). Comparing emission energies, $[(bpy)_2Os(\mu\text{-bbpe})Os(bpy)_2]^{4+*}$ is long-lived compared to $[Os(dmb)_3]^{2+}$.

The extended lifetimes can be explained by invoking the energy gap law which in its simplest form is given by

$$k_{nr} \propto \exp(-S_M) \exp(-\gamma E_0/\hbar\omega_M) \qquad (14)$$

(55) (a) Hoggard, P. E.; Porter, G. B. *J. Am. Chem. Soc.* **1978**, *100*, 1457. (b) Wallace, W. M.; Haggard, P. E. *Inorg. Chem.* **1980**, *19*, 2141. (c) Van Houten, J.; Watts, R. J. *Inorg. Chem.* **1978**, *17*, 3881. (d) Van Houten, J.; Watts, R. J. *J. Am. Chem. Soc.* **1976**, *98*, 4853.

Table 4. Ground State Raman Band Energies (cm^{-1}) in CH_3CN[a]

$[Ru(dmb)_3]^{2+}$ (457.9 nm)	$[Ru(bpy)_2(dmb)]^{2+}$ [b] (457.9.0 nm)	$[(dmb)_2Ru(\mu\text{-bbpe})Ru(dmb)_2]^{4+}$ (488.0 nm)	$[(bpy)_2Os(\mu\text{-bbpe})Os(bpy)_2]^{4+}$ (530.9 nm)	$[Os(bpy)_3]^{2+}$ (488 nm)	ligand assignments[c]
1021	1025	1021	1022	1025	dmb, bpy, bbpe
			1046	1044	bpy
1055					dmb
			1107	1107	bpy
1117		1121			dmb
		1186	1186		bbpe
1193	1201				dmb
		1215	1216		bbpe
1257	1258	1256	1257	1261	dmb, bpy
1269	1274	1273	1272	1268	dmb, bpy, bbpe
1315	1319	1319	1318	1319	dmb, bpy, bbpe
		1329	1335		bbpe
		1425	1425		bbpe
1480	1482	1482	1481	1485	dmb, bpy, bbpe
		1540	1531		bbpe
1547	1550	1550	1553	1554	dmb, bpy, bbpe
1615	1619	1609	1606	1605	dmb, bpy, bbpe
		1638	1638		bbpe

[a] Excitation wavelengths are listed below each complex present as PF_6^- salts at 1×10^{-3} M. [b] Mabrouk, P. A.; Wrighton, M. S. *Inorg. Chem.* **1986**, *25*, 526. [c] The ligand or ligands responsible for the bands at the frequencies indicated. These were summarized by comparisons amongst the complexes and by variations in band intensities with excitation wavelength.

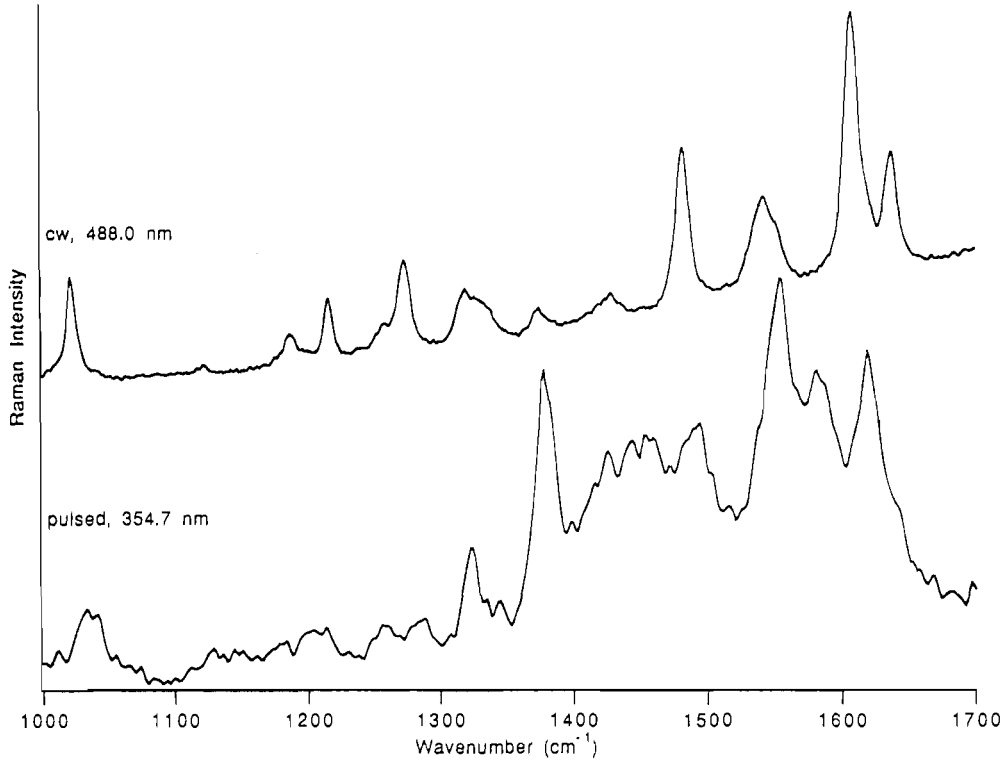

Figure 10. Ground state resonance Raman spectrum of $[(dmb)_2Ru(\mu\text{-bbpe})Ru(dmb)_2](PF_6)_4$ in CH_3CN with 488.0 nm excitation compared to the transient spectrum obtained with 354.7 nm excitation.

where

$$\gamma = \ln(E_0/S_M\hbar\omega_M) - 1 \qquad (15)$$

and $k_{nr} \sim \tau^{-1}$. It is valid in this form if $E_0 \gg h\omega_M$, $S_M\hbar\omega_M \gg k_BT$, and vibrational quantum spacings are the same in excited and ground states, $\hbar\omega_M = \hbar\omega'_M$. Contributions by low frequency modes and the solvent are assumed to remain constant, as is the vibrationally induced electronic coupling matrix element which interconverts the states.[3a,9,12] The electron-vibrational coupling constant, S_M, and quantum spacing are for an average of the several ν(bpy) or ν(bbpe) vibrations that serve as energy acceptors. The energy gap term E_0 is related to E_{00} in Table 2 by

$$E_0 = E_{00} + S_L\hbar\omega_L$$

From the data in Table 2, for $[Ru(bpy)_2(py)Cl]^{+*}$ ($S_M = 0.72$, $\gamma = 1.7$) and $[(dmb)_2Ru(\mu\text{-bbpe})Ru(dmb)_2]^{4+*}$ ($S_M = 0..39$, $\gamma = 2.2$) the term $e^{-S_M}e^{-\gamma E_0/\hbar\omega_M}$ is decreased by ~50 for $[(dmb)_2Ru(\mu\text{-bbpe})Ru(dmb)_2]^{4+*}$ compared to $[Ru(bpy)_2pyCl]^{+*}$. The experimental lifetime ratio is ~20. The agreement is not exact, but this is expected given the approximations involved. Qualitatively, the energy gap law does predict the correct trend. The orgin of the effect is the decrease in S_M (and ΔQ_e) which decreases vibrational overlap and k_{nr}, Figure 1C.

Delocalization in the Acceptor Ligand. The decrease in

Table 5. Raman Band Energies (cm^{-1}) in CH_3CN[a]

$[(dmb)_2Ru(\mu\text{-bbpe})Ru(dmb)_2]^{4+*}$ (pulsed 354.7 nm)	$[(bpy)_2Os(\mu\text{-bbpe})Os(bpy)_2]^{4+*}$ (pulsed 354.7 nm)	$[Ru(dmb)_3]^{2+*}$[b] (pulsed 354.7 nm)	ligand assignment	$bbpe^{\bullet-}$[c] (cw 568.2 nm)
1033	1029		bbpe*, gs dmb/bpy	1026
		1026	dmb*	
1041	1041		bbpe*	1038
1128	1122		bbpe*, gs dmb/bpy	1129
		1177	dmb*	
1205	1195		bbpe*, gs dmb/bpy	
		1202	dmb*	
1213	1213		bbpe*	
			bbpe*	1244
1259			bbpe*, gs dmb/bpy	1257
	1268		bbpe*, gs dmb/bpy	
		1282	dmb*	
1286			bbpe*	1309
		1321	dmb*	
1324	1322		bbpe*	
1345	1341		bbpe*	1363
1425	1430		bbpe*	1433
	1434		bbpe*	
1443	1443		bbpe*	1446
		1445	dmb*	
1456	1463		bbpe*	
1481	1485		bbpe*, gs dmb/bpy	1480
1493	1490		bbpe*	1497
		1496	dmb*	
1554	1555		bbpe*, gs dmb/bpy	1560
		1572	dmb*	
1578			bbpe*	1575
1585	1583(sh)		bbpe*	1594 (sh)
1618	1606		g.s. dmb/bpy	
		1624	dmb*	

[a] The abbreviation sh is for shoulder; bbpe* for an excited state Raman band, and gs dmb/bpy for a a ground state dmb or bpy band that appears in the transient Raman spectrum. Both excitation and Raman scattering were at 354.7 nm for the pulsed experiments. [b] Mabrouk, P. A.; Wrighton, M. S. *Inorg. Chem.* **1986**, *25*, 526. [c] The bbpe radical anion was generated electrochemically in 0.2 M $LiClO_4$ in THF at a platinum grid working electrode, see text.

S_M and ΔQ_e for $[(dmb)_2Ru(\mu\text{-bbpe})Ru(dmb)_2]^{4+*}$ and $[Ru(dmb)_2(bbpe)]^{2+*}$ can be placed on a more intuitive basis by recalling that ΔQ_e for the averaged acceptor mode is related to the changes in local bond displacements ($q_e^* - q_e$) by[13c]

$$\Delta Q_e = [\sum_{j=1}^{b}(q^*_e - q_e)_j^2]^{1/2} \quad (16)$$

The sum is over the local C−C and C−N bonds in the excited, q_e^*, and ground states, q_e. The dimensionless displacements are related to the average bond displacement, $\Delta\bar{r}$, by

$$\Delta\bar{r}^2 = 2\left(\frac{\hbar}{M\omega b}\right)S = \frac{1}{b}(\Delta Q_e)^2 \quad (17)$$

As an illustrative calculation, by using 13 for the reduced mass (M) for a −C=C− in plane ring breathing mode, $b = 13$ for bpy and $b = 29$ for bbpe, $\Delta\bar{r} = 0.013$ Å for $[Ru(bpy)_2(py)Cl]^{+*}$ and 0.006 Å for $[(dmb)_2Ru(\mu\text{-bbpe})Ru(dmb)_2]^{4+*}$ in 4:1 (v:v) EtOH−MeOH at 157 K.

Evidence for decreased displacements at bbpe also appear in the resonance Raman data in Tables 4 and 5. A mode by mode comparison reveals that excited to ground state frequency shifts are considerably less for bbpe in $[(dmb)_2Ru(\mu\text{-bbpe})Ru(dmb)_2]^{4+*}$ than for dmb in $[Ru(dmb)_3]^{2+*}$. For $[Ru(dmb)_3]^{2+}$ the ground to excited state shifts are $\Delta\bar{\nu} = -57$ cm^{-1} for the band at 1615 cm^{-1} and +10 cm^{-1} for the band at 1117 cm^{-1}. For $[(dmb)_2Ru(\mu\text{-bbpe})Ru(dmb)_2]^{4+*}$ the shifts are $\Delta\bar{\nu} = -24$ cm^{-1} for the 1609 cm^{-1} band and +6 cm^{-1} for the 1121 cm^{-1} band.

The decreased displacements are consistent with delocalization. Delocalization causes more bonds to be distorted, but the *average* distortion at each bond is decreased. The effect is magnified in k_{nr} since S varies with the *square* of $\Delta\bar{r}$.

These arguments are qualitative. The AM1 calculations show that the detailed changes between bbpe and $bbpe^{\bullet-}$ may be quite complicated. For example, the bpy's in bbpe are canted (Figure 3, $\theta = 22.7°$), while the bpy's in $bbpe^{\bullet-}$ are flat ($\theta = 0°$) to maximize delocalization of the added electron.

Radiative Decay. The orbital coefficients in the LUMO of $bbpe^{\bullet-}$ vary with θ. When $\theta \neq 0°$, the p_x, p_y, and p_z orbitals at the N atoms nearest the double bond all contribute. At $\theta = 0°$, the lowest π^* orbitals are primarily p_z. The orbital description of the LUMO resembles *trans*-1,2-bis-4,4′-bipyridyl ethene (bpe) with the distal pyridyl rings acting as substituents. In the anion this effect is even more pronounced. Localization in selected positions of other unsymmetrical polypyridine ligands has been reported in other ligand-bridged complexes.[56]

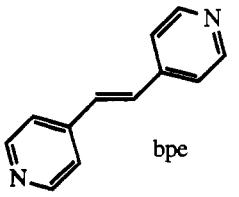

bpe

The electronic asymmetry may play a role in radiative decay. Both $[Ru(dmb)_2(bbpe)]^{2+*}$ and $[(dmb)_2Ru(\mu\text{-bbpe})Ru(dmb)_2]^{4+*}$ are weak emitters; k_r is decreased by 10−20 compared to $[Ru(dmb)_3]^{2+*}$. k_r is related to the square of the transition dipole moment ($\langle\vec{\mu}\rangle$) and the cube of the average emission energy ($\langle\bar{\nu}^{-3}\rangle^{-1}$) by[3a,57]

$$k_r \propto \langle\vec{\mu}\rangle^2\langle\bar{\nu}^{-3}\rangle^{-1} \quad (18)$$

(56) Cooper, T. B.; MacQueen, D. B.; Petersen, T. D.; Wertz, D. W. *Inorg. Chem.* **1990**, *29*, 3701.

The transition dipole moment is given by

$$\langle \vec{\mu} \rangle = \langle \Psi_{es} | e\vec{r} | \Psi_{gs} \rangle$$

where Ψ_{gs} and Ψ_{es} are the electronic wave functions for the ground and excited states and $\vec{r}$ is the vector displacement of the excited electron. For an LMCT, $d\pi \rightarrow \pi^*$ emission

$$\langle \vec{\mu} \rangle = \langle \psi_{\pi^*} | e\vec{r} | \psi_{d\pi} \rangle$$

where ψ_{π^*} and $\psi_{d\pi}$ are the electronic wave functions for the π^* acceptor and $d\pi$ donor orbitals. By using the LCAO approximation for ψ_{π^*}, neglecting nonadjacent overlap, and defining $\psi_{d\pi} = d\pi$ to be the orbital containing the hole, the transition dipole moments for $[Ru(dmb)_3]^{2+*}$ and $[(dmb)_2Ru(\mu\text{-bbpe})Ru(dmb)_2]^{4+*}$ are given by

$$\langle \vec{\mu}_{dmb} \rangle = 2a_N \langle p_N | e\vec{r} | d\pi \rangle \quad (19a)$$

$$\langle \vec{\mu}_{bbpe} \rangle = a'_N \langle p'_N | e\vec{r} | d\pi \rangle \quad (19b)$$

The p_N, p'_N and a_N, a'_N are the wave functions and coefficients in π^*. There are two contributing orbitals for dmb but because of the electronic asymmetry in $bbpe^{\bullet-}$ (Figure 3), there is effectively only one for bbpe.

From eqs 18 and 19 the ratio of k_r's is

$$\frac{k_{r,bbpe}}{k_{r,dmb}} = \frac{\langle \vec{\mu}_{bbpe} \rangle^2 \langle \bar{\nu}_{bbpe}{}^{-3} \rangle^{-1}}{\langle \vec{\mu}_{dmb} \rangle^2 \langle \bar{\nu}_{dmb}{}^{-3} \rangle^{-1}} = \left(\frac{a_N'}{2a_N}\right)^2 \left(\frac{1}{1.13}\right) = 0.3$$

This estimate was made by assuming that the transition dipole moment integrals have the same magnitude, evaluating the energy gap ratio (=1/1.13), and by using the orbital coefficients in Figure 3. It is a lower limit since it is expected that the electronic asymmetry in $bbpe^{\bullet-}$ may account for part of the experimental decrease in $k_{r,bbpe}$, but a minor part. A similar effect has been observed for radiative decay in $[(dmb)(CO)_3Re(4,4'\text{-bpy})Re(CO)_3(bpy)]^{2+*}$ where 4,4′-bpy is the acceptor ligand.[52b]

Conclusions

In the lowest MLCT excited states of $[(dmb)_2Ru(\mu\text{-bbpe})Ru(dmb)_2]^{4+}$, $[Ru(dmb)_2(bbpe)]^{2+}$, and probably $[(bpy)_2Os(\mu\text{-bbpe})Os(bpy)_2]^{4+}$ the excited electron is delocalized to a substantial degree over the π^* framework of bbpe. Delocalization decreases displacement changes, vibrational overlap, and k_{nr}. This is an important conclusion for the design of MLCT excited states. An extended π^* system in the acceptor ligand should lead to extended excited state lifetimes and may allow for the preparation of "black" absorbers having accessible excited state lifetimes. These shifts to the red, of course, come with a decrease in excited state redox potentials. On the basis of the E_{00} values in Table 2, the couples $[(dmb)_2Ru(\mu\text{-bbpe})Ru(dmb)_2]^{4+*/3+}$ and $[(dmb)_2Ru(\mu\text{-bbpe})Ru(dmb)_2]^{5+/4+*}$ are decreased in magnitude by ~0.3 V compared to the couples $[Ru(dmb)_3]^{2+*/+}$ and $[Ru(dmb)_3]^{3+/2+*}$.

Although not generally recognized as such in the literature, the "delocalization effect" may be common. For example, for 2,2′:4′,4″:2″,2‴-quaterpyridine (QPY)[58] or 2,2-bis(2′-pyridyl)-benzo[g]quinoxaline (DPB)[59] as an acceptor, extended lifetimes and red-shifted emissions are observed as well.

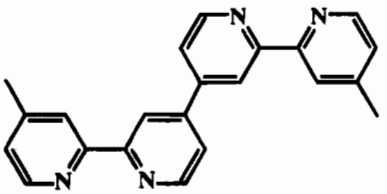

QPY

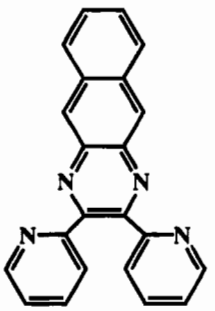

DPB

Acknowledgment. Acknowledgments are made to the Department of Energy under Grant No. DE-FG05-86ER 13633 for support of this work and the SERC for postdoctoral support for S.B.

Supplementary Material Available: Figures showing the spectroelectrochemical results of one-electron reduction of bbpe and $[(bpy)_2Os(\mu\text{-bbpe})Os(bpy)_2]^{4+}$, transient absorption difference spectra for $[Ru(dmb)_3](PF_6)_2$ $[Ru(dmb)_2(vbpy)](PF_6)_2$ and $[Os(bpy)_2(bbpe)](PF_6)_2$ in CH_3CN, and simulated excited state absorption spectra for $[(dmb)_2Ru(\mu\text{-bbpe})Ru(dmb)_2](PF_6)_4$ and $[(bpy)_2Os(\mu\text{-bbpe})Os(bpy)_2](PF_6)_4$ and supplemental tables for the Z-matrix output file from AM1 calculations on bbpe, $bbpe^{\bullet-}$, dmb, and $dmb^{\bullet-}$ (11 pages). Ordering information is given on any current masthead page.

IC9409571

(57) The term $\langle \bar{\nu}^{-3} \rangle^{-1}$ can be calculated from the ratio

$$\langle \bar{\nu}^{-3} \rangle^{-1} = (\int I(\bar{\nu})\, d\bar{\nu}) / (\int I(\bar{\nu}) \bar{\nu}^{-3} / d\bar{\nu})$$

where I is the emission intensity in units of quanta per energy interval per second.[3a] Experimentally, it can be estimated as the cube of the emission energy.

(58) Downard, A.; Steel, P. *Inorg. Chem.* **1991**, *30*, 2259.
(59) Baiano, J. A.; Murphy, W. R., Jr. *Inorg. Chem.* **1991**, *30*, 4594.